

# Characteristics and sources of VOCs and the O<sub>3</sub>-NO<sub>x</sub>-NMVOCs relationships in Zhengzhou, China

Dong Zhang<sup>1,3</sup>, Xiao Li<sup>2,3</sup>, Minghao Yuan<sup>4</sup>, Yifei Xu<sup>4</sup>, Qixiang Xu<sup>2,3</sup>, Fangcheng Su<sup>2,3</sup>, Shenbo Wang<sup>2,3</sup>,  
Ruiqin Zhang<sup>2,3,\*</sup>

1 College of Chemistry, Zhengzhou University, Zhengzhou 450001, China

2 School of Ecology and Environment, Zhengzhou University, Zhengzhou, 450001, China

3 Institute of Environmental Sciences, Zhengzhou University, Zhengzhou 450001, China

4 Environmental Protection Monitoring Center Station of Zhengzhou, Zhengzhou 450007, China

**Correspondence:** Ruiqin Zhang (rqzhang@zzu.edu.cn)

## Abstract:

**Nonmethane volatile organic compounds (NMVOCs)** are important precursors of ozone (O<sub>3</sub>) generation. Understanding the characteristics, and emission sources of NMVOCs, and the relationship between NMVOCs and O<sub>3</sub> during O<sub>3</sub> pollution are of great significance for O<sub>3</sub> pollution control. This study investigated the characteristics, sources, and effects of NMVOCs on O<sub>3</sub> formation in Zhengzhou, Henan Province from 1<sup>st</sup> to 30<sup>th</sup> June 2023, and provided recommendations for O<sub>3</sub> emission reduction strategies. Two O<sub>3</sub> pollution events occurred during the observation period. During the observation period, the concentration of **Total NMVOCs (TNMVOCS)** varied from 9.9 to 60.3 ppbv, with an average of  $22.8 \pm 8.3$  ppbv. The average concentration of TNMVOCS in the two pollution events were higher than that on the clean days. Six major NMVOCs sources were identified by using the Positive Matrix Factorization model. Vehicular exhaust (28%), solvent usage (27%), and industrial production (22%) were the main sources. An observation-based mode was applied to explore the O<sub>3</sub>-precursors relationship and observation-oriented O<sub>3</sub> control strategies. The results of relative incremental reactivity (RIR) and empirical kinetics modeling approach showed that the O<sub>3</sub> formation in Zhengzhou in June was in anthropogenic VOCs (AVOCs)-limited **regime**. NMVOCs with the largest RIR values, while NO<sub>x</sub> had a negative RIR value. It was worth noting that the sensitivity of O<sub>3</sub> generation to biogenic VOCs (BVOCs) was greater than that of AVOCs. From the perspective of the reduction effect, the reduction ratios of AVOCs/NO<sub>x</sub> should be no less than 3:1, which was conducive to the reduction of O<sub>3</sub> formation.

**Keywords:** Emission reduction strategies; Positive Matrix Factorization; Relative incremental reactivity; The observation-based model; Empirical kinetics modeling approach

## 1 Introduction

In recent years, ozone (O<sub>3</sub>) pollution has become increasingly prominent in China, especially in urban areas (Liu et al., 2023a; Zhao et al., 2021; Yan et al., 2023; Sicard et al., 2020). O<sub>3</sub> pollution has become an important factor affecting the ambient air quality (Zhang et al., 2023). Nonmethane volatile organic compounds (NMVOCs), as an important precursor of O<sub>3</sub> and secondary organic aerosols, widely exist in the atmospheric environment and participate in many photochemical reactions, which have an important impact on atmospheric oxidation capacity and air quality (Zhu et al., 2021). Some NMVOCs are also air toxics (Billionnet et al., 2011), such as benzene, trichloroethylene, and chloroform (Lerner et al., 2012). Long-term exposure to higher concentrations of NMVOCs can lead to acute or chronic risks (He et al., 2015). Therefore, it is necessary to continue to carry out NMVOCs monitoring activities in O<sub>3</sub> pollution areas to analyze O<sub>3</sub> concentration levels, sources, and effects on O<sub>3</sub> generation.

The concentration of NMVOCs is affected by background concentration, weather conditions (Mo et al., 2015), emission sources, terrain conditions (Liu et al., 2016), and extent of pollutant transport (Shao et al., 2009). In addition, under meteorological conditions with higher temperature, NMVOCs exhibit photochemical losses during dispersion and regional transport (Zou et al., 2023; Liu et al., 2023a; Liu et al., 2020). **As a result, the ambient NMVOCs concentration varies with the locality and season.** For example, in typical coastal areas of Ningbo, the seasonal variation of NMVOCs concentration was winter > spring > Autumn > summer (Huang et al., 2023). The coastal areas of Shandong Province had the highest value in winter ( $28.5 \pm 15.1$  ppbv) and the lowest value in autumn ( $14.5 \pm 7.6$  ppbv) (Huang et al., 2023). The average summer TNMVOCs concentration in the suburbs of Jinan ( $12.0 \pm 5.1$  ppbv) (Liu et al., 2023c) was lower than that in the suburbs of Beijing ( $18.3 \pm 8.9$  ppb), and much lower than that in the central city of Beijing ( $44.0 \pm 28.9$  ppbv) (Wu et al., 2023). The average TNMVOCs concentration ( $21.7$  ppbv) in the O<sub>3</sub> pollution period in Tianjin is 12% higher than that in the non-O<sub>3</sub> pollution period (Liu et al., 2023a).

NMVOCs are emitted from various sources including anthropogenic sources and biogenic sources (Chameides et al., 1992) as well as secondary generation through photochemical reactions (Yuan et al., 2012). The main sources of NMVOCs include motor vehicle emissions, industrial processes, solvent usage, fuel evaporation, combustion, and biogenic emissions (Wu et al., 2016; Prendez et al., 2013; Watson et al., 2001). Biogenic emission is mainly affected by temperature and radiation conditions (Li et al., 2020). Biogenic emissions are therefore higher during hotter months, especially in summer (Pacifico et al., 2009; Xu et al., 2023). Urban areas are greatly affected by anthropogenic sources (Zhang et al., 2023; Goldstein and Galbally, 2007). In different regions, the main contribution sources of NMVOCs are different. For example, the main

anthropogenic VOCs (AVOCs) sources in the Yangtze River Delta region of China are vehicle and solvent evaporation (Xu et al., 2023). The Pearl River Delta region is mainly affected by solvent use, liquefied petroleum gas use, and vehicle exhaust. Atmospheric NMVOCs in Beijing are greatly affected by motor vehicle emission sources and combustion sources (Liu et al., 2021; Zhang et al., 2020). Huang et al. (2023) reported that plastic synthesis, industrial processes, organic solvents, dyeing, traffic emissions, and pesticides were identified as the main sources of NMVOCs in Ningbo City in the coastal area (Liu et al., 2023b). Since different emission sources have different contributions to NMVOCs and thus have different impacts on the generation of O<sub>3</sub> (Zhang et al., 2023), it is necessary to investigate the sources of NMVOCs in different cities. Designing a reasonable and effective precursor emission control strategy is crucial to control the photochemical generation of O<sub>3</sub> (Yang et al., 2021). The relationship between O<sub>3</sub> and precursors is nonlinear (Chameides et al., 1992), and precursor emission reduction strategies need to be dynamically adjusted based on the actual sensitivity of O<sub>3</sub> formation (Chu et al., 2023; Lin et al., 2005). The observation-based model (OBM) is a widely used tool to analyze O<sub>3</sub>-NO<sub>x</sub>-NMVOCs sensitivity (Zhang et al., 2008; Nelson et al., 2021; Cardelino and Chameides, 1995). Several studies in China have analyzed the sensitivity of O<sub>3</sub> to precursors and control scenarios. For example, O<sub>3</sub> in the central area of the Yangtze River Delta is in a NMVOCs-limited regime, and AVOCs play a leading role in the formation of O<sub>3</sub> (Liu et al., 2023b). Chengdu is in a typical NMVOCs restricted area, so NMVOCs emission reduction helps to prevent and control O<sub>3</sub> pollution, and the emission reduction scenario based on NMVOCs source showed that the emission reduction ratio of NMVOCs to NO<sub>2</sub> needs to reach more than 3 to achieve prevention of O<sub>3</sub> pollution (Chen et al., 2022b). Xie et al. (2021) found that controlling NMVOCs in Leshan, a non-provincial capital city in southwest China, can effectively reduce the photochemical generation of O<sub>3</sub>, and pointed out that the best emission reduction strategy for NMVOCs and NO<sub>x</sub> should be 3:1. In addition, the generation of O<sub>3</sub> in areas such as Shanghai (Lu et al., 2023), Rizhao (Zhang et al., 2023), and Nanjing (Mozaffar et al., 2021) is generally limited by NMVOCs. However, in the United States and European countries, O<sub>3</sub> formation gradually transitioned from NMVOCs-limited regime to NO<sub>x</sub>-limited regime (Nopmongcol et al., 2012; Ring et al., 2018; Goldberg et al., 2016).

Zhengzhou is the capital city of Henan Province and an important transportation hub in China. High population density levels, large vehicle ownership (MPS, 2022) and complex industrial structures determine the complexity of NMVOCs emission sources. In recent years, Zhengzhou's O<sub>3</sub> pollution has increasingly intensified, becoming one of the cities with the highest O<sub>3</sub> pollution in central China (Wang et al., 2023b; Min et al., 2022). From 2020 to 2022, the annual 90th percentile of the mean daily maximum 8 h average O<sub>3</sub> (O<sub>3</sub>-8H-90per) published by Zhengzhou Ecological Environment Bureau were 182, 177 and 178 μg/m<sup>3</sup>,

91 respectively, which were 10% to 13% higher than the National Ambient Air Quality Grade II Standard (160  
92  $\mu\text{g}/\text{m}^3$ ) (<https://sthjj.zhengzhou.gov.cn/>, last access: June, 2023). Some studies have analyzed the  
93 concentration levels, sources, and impact of NMVOCs on  $\text{O}_3$  in Zhengzhou (Zeng et al., 2023; Wang et al.,  
94 2023b; Min et al., 2022). Wang et al. (2022) analyzed the sensitivity of  $\text{O}_3$  to precursors and found that in July  
95 with low  $\text{O}_3$  levels in Zhengzhou,  $\text{O}_3$  formation was in a **NMVOCs-limited regime**, while on  $\text{O}_3$  pollution  
96 accumulation and persistence days,  $\text{O}_3$  formation was in a transitional state. Yu et al. (2021) showed that  
97 Zhengzhou was under a **NMVOCs-sensitive regime** in September. The above studies all show that it is  
98 important to study the emission reduction of precursors to control  $\text{O}_3$  generation. However, there is still a lack  
99 of relevant research on June, the month with the **highest**  $\text{O}_3$  pollution in Zhengzhou. In order to effectively  
100 solve the increasingly serious trend of  $\text{O}_3$  pollution in Zhengzhou, it is necessary to give priority to and  
101 strengthen the research of Zhengzhou area, especially during the period of high  $\text{O}_3$  pollution. Therefore, it is  
102 necessary to continue to pay attention to the pollution levels of  $\text{O}_3$  and precursors in Zhengzhou and further  
103 explore the relationship between them.

104 In this study, we conducted an online measurement of NMVOCs in June, when  $\text{O}_3$  pollution was severe in  
105 Zhengzhou. The concentration, composition, and diurnal variation of NMVOCs in the atmosphere were  
106 analyzed. The main sources of NMVOCs were discussed by using ratio method and Positive Matrix  
107 Factorization (PMF) model. OBM was used to analyze the sensitivity of  $\text{O}_3$ -NMVOCs- $\text{NO}_x$  and consequently  
108 the emission reduction strategy of precursors to control  $\text{O}_3$  concentration was proposed. This study establishes  
109 a collaborative control strategy for atmospheric NMVOCs, which is of great significance for the control of  
110 atmospheric  $\text{O}_3$  pollution in Zhengzhou.

## 111 **2. Materials and methods**

### 112 **2.1 Sampling site**

113 The monitoring site is on the roof (about 20 m above ground) of the building at Zhengzhou Environmental  
114 Protection Monitoring Centre Station (34.75° N, 113.60° E) (Fig. S1). **The sampling site is a typical urban site,**  
115 **surrounded by residential areas, commercial areas, and office buildings. There are no point sources of air**  
116 **pollution nearby within a radius of 1 meter. The sampling site may be affected by motor vehicle and plant**  
117 **emissions.**

### 118 **2.2 Sample collection and chemical analysis**

119 The sampling campaign was conducted from 1<sup>st</sup> to 30<sup>th</sup> June 2023. NMVOCs concentrations were observed  
120 with a gas chromatography-mass spectrometer, GC-MS (TH-PKU 300B, Wuhan Tianhong Instrument, China),  
121 which adopted detection technology of ultralow-temperature preconcentration combined with GC-MS/ flame

ionization detector (FID). The time resolution of the instrument is 1 hour, and the flow rate is 60 mL/min. The air sample was collected for the first 5 minutes of each hour and then pre-concentrated through a cold trap to remove H<sub>2</sub>O<sub>2</sub> and CO<sub>2</sub>. The sample was captured using an empty capillary column. After pre-concentration, the sample was desorbed by rapid heating and introduced into an analytical system. After separation by chromatographic column, the sample was detected by FID (for C<sub>2</sub>-C<sub>5</sub> hydrocarbons) and MS (for C<sub>5</sub>-C<sub>12</sub> hydrocarbons, halocarbons and OVOCs). The correlation coefficient of the standard curve of the target compound was greater than or equal to 0.99, and the detection limit of the instrument method was less than or equal to 0.1 nmol/mol. A total of 115 NMVOCs were monitored, including 29 alkanes, 11 alkenes, 1 alkyne, 17 aromatic hydrocarbons, 35 halogenated hydrocarbons, 21 OVOCs and 1 sulfide (carbon disulfide). Details of the device can be found in our previous study (Zhang et al., 2021). The individual NMVOCs concentration measured during the observation period is shown in Table S1. Also the study conducted the simultaneous online measurements of hourly concentrations of particulate matter (PM<sub>2.5</sub> and PM<sub>10</sub>), other trace gases (CO, O<sub>3</sub>, NO, and SO<sub>2</sub>), and meteorological data (temperature (T), relative humidity (RH), atmospheric pressure, and wind speed (WS) and wind direction (WD)).

### 2.3 PMF model

The PMF 5.0 is an advanced multivariate factor analysis tool (USEPA, 2014), which can be used to identify the sources of NMVOCs (Norris et al., 2014). PMF model is expressed as follows:

$$X_{ij} = \sum_{k=1}^p g_{ik} f_{kj} + e_{ij} \quad (1)$$

where, i, j, and k represent the i<sup>th</sup> sample, the j<sup>th</sup> chemical species, and the k<sup>th</sup> factor, respectively; X represents the chemical species concentration measured in the sample; g is the species contribution; f is the species fraction; and e is the residual matrix.

The number of factors is obtained by minimizing objective residual function Q: as follows:

$$Q = \sum_{i=1}^n \sum_{j=1}^m \left[ \frac{X_{ij} - \sum_{k=1}^p g_{ik} f_{kj}}{u_{ij}} \right]^2 \quad (2)$$

Where  $\mu_{ij}$  is the sample data uncertainty.

The sample data uncertainty is calculated by Equations (3) and (4). If the data concentration is less than method detection limit (MDL), Equation (3) is used. Otherwise, Equation (4) is used.

$$\text{Unc} = \frac{5}{6} \times \text{MDL} \quad (3)$$

$$\text{Unc} = \sqrt{(\text{Error Fraction} \times \text{concentration})^2 + (0.5 \times \text{MDL})^2} \quad (4)$$

where Error Fraction represent the precision (%) of each species;

Species with high proportions of missing samples or concentration values more than 25% below MDLs were excluded, while NMVOCs serving as typical tracers of emission sources were included (USEPA, 2014), and NMVOCs with short atmospheric lifetimes were excluded (Callén et al., 2014; Guo et al., 2011). In this study, 29 out of 115 NMVOCs collected over the sampling period was analyzed by the PMF model. In this study, a seven-factor solution ( $Q_{\text{true}}/Q_{\text{theoretical}} = 3.42$ ; and  $F_{\text{peak}} = 0$ ) was chosen (Fig. S2).

## 2.4 Conditional probability function analysis

The conditional probability function (CPF) is a source identification tool, which can be used to identify local emission sources of pollutants (Uria-Tellaetxe and Carslaw, 2014). CPF analysis methods were employed to determine the potential direction of emission sources by utilizing the wind directions and source contributions calculated through PMF (Kim and Hopke, 2004). The CPF is defined as:

$$\text{CPF} = \frac{m_{\Delta\theta}}{n_{\Delta\theta}} \quad (5)$$

the variable  $m_{\Delta\theta}$  represents the frequency of occurrences from the wind sector  $\Delta\theta$  for the top 75% contributions of each identified NMVOCs source, while  $n_{\Delta\theta}$  represents the total occurrences from the same wind sector. CPF analysis were constructed using the 'openair' package (Carslaw and Ropkins, 2012) in the statistical software R (R Foundation for Statistical Computing, Vienna, Austria).

## 2.5 OBM

OBM based on the Master Chemical Mechanism (MCM v3.3.1; <https://mcm.york.ac.uk/MCM/>) was employed to estimate the effect of changes of what in  $O_3$  precursors (Liu et al., 2022). Detailed information about OBM can be viewed in previous studies (Chu et al., 2023; Ling et al., 2011). Briefly, OBM assumes a good mix of emitted pollutants and is independent of emission inventories and meteorological data, combined with atmospheric chemical mechanisms, simulates the  $O_3$  production rate and the corresponding  $O_3$  concentration at a given time (Kleinman, 2000; Qiao et al., 2023). In this model, the net production rate  $O_3$  ( $P(O_3)$ ) is the difference between the  $O_3$  production (the oxidation of NO by  $HO_2$  and  $RO_2$ ) and  $O_3$  destruction ( $O_3$  photolysis, reactions of  $O_3$  with OH and  $HO_2$ , reactions of OH with  $NO_2$ , and reactions of  $O_3$  with alkenes). This method for estimating  $O_3$  production and removal rates has been utilized in several previous studies (Wang et al., 2017; Wang et al., 2022). The constants (k) represent the rate coefficients of the respective reactions, as follows:

$$P(O_3) = k_{HO_2+NO}[HO_2][NO] + \sum k_{RO_2i+NO}[RO_{2i}][NO] - k_{HO_2+O_3}[HO_2][O_3] - k_{OH+O_3}[OH][O_3] -$$



$$k_{O(^1D)+H_2O}[O(^1D)][H_2O] - k_{OH+NO_2}[OH][NO_2] - k_{alkenes+O_3}[alkenes][O_3] \quad (6)$$

The relative incremental reactivity (RIR) was computed through OBM to evaluate the sensitivity of the photochemical production of O<sub>3</sub> to changes in the concentration of individual precursors within a given region (Ling et al., 2013; Cardelino and Chameides, 2000), which can be calculated from Eq. (7):

$$RIR(X) = \frac{[P_{O_3}(X) - P_{O_3}(X - \Delta X)]/P_{O_3}(X)}{\Delta S(X)/S(X)} \quad (7)$$

where X is the specific precursor of O<sub>3</sub>; P<sub>O<sub>3</sub></sub>(X) and P<sub>O<sub>3</sub></sub>(X - ΔX) are the net production of O<sub>3</sub> simulated by the OBM; and ΔS(X)/S(X) is the change in the concentration of S(X). The large change in primary pollutants (>20%) deviates greatly from the base scenario and is not representative of the current situation. Therefore, the concentration changes of ΔS(X)/S(X) were assumed to be 20%. In this study, the S for NMVOCs and NO<sub>x</sub> were reduced by 0-100%. The relative change of P<sub>O<sub>3</sub></sub>(X) with S(NMVOCs) and S(NO<sub>x</sub>) can be expressed by the isogram of P<sub>O<sub>3</sub></sub>(X).

The concentrations of trace gases (SO<sub>2</sub>, O<sub>3</sub>, CO, and NO), and meteorological parameters (T, RH, and WS) with 1 h time resolution were used as constraints in this model. At the same time, the concentrations of 75 NMVOCs observed with 1 h time were selected for input into the model because these 75 NMVOCs were included in MCM v3.3.1. The photolysis frequency (J(H<sub>2</sub>O<sub>2</sub>), J(NO<sub>2</sub>)) and planetary boundary layer are the default values. Then, the differential equation is calculated with a time resolution of 1 h, and the mixing proportion of various photochemical reaction products, intermediates and free radicals can be obtained.

To evaluate the performance of this model, the index of agreement (IOA) was used in this study (Huang et al., 2005):

$$IOA = 1 - \frac{\sum_{i=1}^n (O_i - M_i)^2}{\sum_{i=1}^n (|O_i - \bar{O}| + |M_i - \bar{O}|)^2} \quad (8)$$

where O<sub>i</sub>, M<sub>i</sub>, and  $\bar{O}$  represent the hourly values of observation, the simulation, and the average of observations, respectively. In various studies, model simulation results are often considered acceptable when the value of IOA falls within the range of 0.68 to 0.89 (Wang et al., 2018). To evaluate the reliability of our model simulations, we conducted an analysis of O<sub>3</sub> concentration in the atmosphere and calculated the IOA value. Our model does not directly incorporate O<sub>3</sub> observations. Instead, it utilizes concentrations of trace gases (SO<sub>2</sub>, CO, and NO) and 75 NMVOCs, and meteorological parameters (T, RH, and WS) to simulate the concentration of O<sub>3</sub> in the atmospheric environment. The IOA values for O<sub>3</sub> was calculated from 7:00 to 19:00 during the day and obtained a result of 0.8. Therefore, the results simulated by our model are reliable.

## 3 Results and discussions

### 3.1 General characteristics

#### 3.1.1 NMVOCs concentrations and composition

According to the national ambient air quality standard (NAAQS-2012) of China (Ministry of Environmental Protection of China, 2012), the grade II threshold of the maximum daily 8-h average (MDA8) of O<sub>3</sub> was 160 µg/m<sup>3</sup> (~75 ppbv). Two O<sub>3</sub> pollution events were found over 160 µg/m<sup>3</sup>, which were named Case 1 (8<sup>th</sup>-17<sup>th</sup> Jun.) and Case 2 (20<sup>th</sup>-27<sup>th</sup> Jun.). Meanwhile, there were also O<sub>3</sub> pollution events on 6<sup>th</sup> Jun. and 29<sup>th</sup>-30<sup>th</sup> Jun. However, for better data coverage, we only discussed periods of O<sub>3</sub> pollution that lasted at least a week, and processes with relatively few days of pollution were not discussed in this study. The rest of the observation periods were clean days. Figure 1 shows the time series of the concentration of TNMVOCs, O<sub>3</sub> 8-h moving average, SO<sub>2</sub>, PM<sub>2.5</sub>, NO<sub>x</sub>, CO, meteorological parameters (WD, WS, T, and RH), and from 1<sup>st</sup> to 30<sup>th</sup> June 2023. The gray areas in Fig. 1 are O<sub>3</sub> pollution events, and the remaining areas are clean days. During the observation, O<sub>3</sub> polluted days were 21 days, accounting for 70%. During the observation period, the average wind speed ( $1.3 \pm 0.9$  m/s) was relatively low, which was not conducive to the dispersion. The mean RH ( $52 \pm 19\%$ ) was low, and the mean temperature ( $28.9 \pm 4.6$  °C) was high. The meteorological conditions of high temperature and low RH were conducive to the occurrence of photochemical pollution. The maximum daily 8-h moving average (MDA8) of O<sub>3</sub> reaching 229 µg/m<sup>3</sup>. Hourly average concentration of SO<sub>2</sub>, NO<sub>2</sub>, CO, and PM<sub>2.5</sub> were  $4.4 \pm 3.3$  µg/m<sup>3</sup>,  $26.5 \pm 17.9$  µg/m<sup>3</sup>,  $0.6 \pm 0.2$  mg/m<sup>3</sup>,  $59.6 \pm 26.5$  µg/m<sup>3</sup> and  $22.9 \pm 7.1$  µg/m<sup>3</sup>, respectively. The concentrations of these pollutants were 97%, 87%, 94%, and 35% lower than the grade I threshold of the NAAQS-2012. The average concentration of TNMVOCs was  $22.8 \pm 8.3$  ppbv.

During the Case 1 process, O<sub>3</sub> pollution continued for 10 days. The average RH and temperature were  $41 \pm 16\%$  and  $29.9 \pm 4.1$  °C, respectively, and the average WS was  $1.3 \pm 0.8$  m/s. The concentration of MDA8 O<sub>3</sub> reached a maximum of 228 µg/m<sup>3</sup> (June 11) during the pollution period, which was higher than the grade II threshold of MDA8 O<sub>3</sub>. In Case 1, the mean concentrations of SO<sub>2</sub>, NO<sub>2</sub>, CO, PM<sub>10</sub> and PM<sub>2.5</sub> were  $6.1 \pm 4.1$  µg/m<sup>3</sup>,  $27.4 \pm 19.5$  µg/m<sup>3</sup>,  $0.6 \pm 0.1$  mg/m<sup>3</sup>,  $69.1 \pm 31.5$  µg/m<sup>3</sup> and  $25.6 \pm 6.8$  µg/m<sup>3</sup>, respectively. The average concentration of TNMVOCs during this process was  $24.1 \pm 8.9$  ppbv. In Case 2, O<sub>3</sub> pollution occurred continuously for 8 days. The average RH and average temperature were  $50 \pm 14\%$  and  $31.2 \pm 2.9$  °C. The average concentrations of TNMVOCs ( $22.5 \pm 7.4$  ppbv), SO<sub>2</sub> ( $2.7 \pm 2.1$  mg/m<sup>3</sup>), NO<sub>2</sub> ( $24.9 \pm 12.3$  mg/m<sup>3</sup>), CO ( $0.6 \pm 0.1$  mg/m<sup>3</sup>), PM<sub>10</sub> ( $61 \pm 19$  mg/m<sup>3</sup>), and PM<sub>2.5</sub> ( $24 \pm 7$  mg/m<sup>3</sup>) in Case 2 were all lower than those



237 in Case 1 process.

238 The average concentrations of TNMVOCs, NO<sub>2</sub>, PM<sub>10</sub>, and PM<sub>2.5</sub> on clean days were lower than those of the  
239 O<sub>3</sub> pollution events. The average RH ( $65 \pm 17\%$ ) on clean days was higher than those during Case 1 and Case  
240 2 events, while the average temperature ( $26.0 \pm 4.8$  °C) was lower than those during Case 1 and Case 2 events.  
241 According to the analysis in Fig. S3a and Fig. S3b, O<sub>3</sub> has a significant correlation with temperature and RH,  
242 with correlation coefficients of 0.7 and -0.61 respectively. Therefore, conditions of high temperature and low  
243 RH are more conducive to O<sub>3</sub> pollution. Fig. S3c indicates that O<sub>3</sub> concentration exceeding the secondary  
244 standard mainly occurs under meteorological conditions of high temperature (greater than 30 °C) and low RH  
245 (less than 55%). It can be noted that when  $35$  °C < T <  $40$  °C and  $20\%$  < RH <  $40\%$ , the O<sub>3</sub> concentration  
246 consistently exceeds the grade II threshold of the NAAQS-2012. High temperature and low RH are more  
247 conducive to O<sub>3</sub> pollution (Chen et al., 2020; Zhang et al., 2015). Meng et al. (2023) argued that most of the  
248 reactions involved in O<sub>3</sub> formation increase with temperature, and the rate of O<sub>3</sub> production exceeds that of  
249 O<sub>3</sub> loss by a large margin. Therefore, during the study period, the meteorological conditions of high  
250 temperature and low RH are also important factors affecting the occurrence of O<sub>3</sub> pollution.

251 Besides, the average concentration of NO<sub>2</sub> in clean days ( $24.4 \pm 16.1$  ppbv) was lower than that in Case 1 and  
252 Case 2, while the average concentration of NO in clean days ( $4.8 \pm 5.5$  ppbv) was higher than that in Case 1  
253 ( $3.9 \pm 3.75$  ppbv) and Case 2 ( $3.9 \pm 2.4$  ppbv). Higher concentration of NO<sub>2</sub> can promote the formation of O<sub>3</sub>,  
254 while the titration reaction between NO and O<sub>3</sub> consumes O<sub>3</sub> (Sillman, 1999). Therefore, the higher  
255 concentration of NO<sub>2</sub> and lower concentration of NO during pollution events are one of the reasons for the  
256 occurrence of O<sub>3</sub> pollution events.

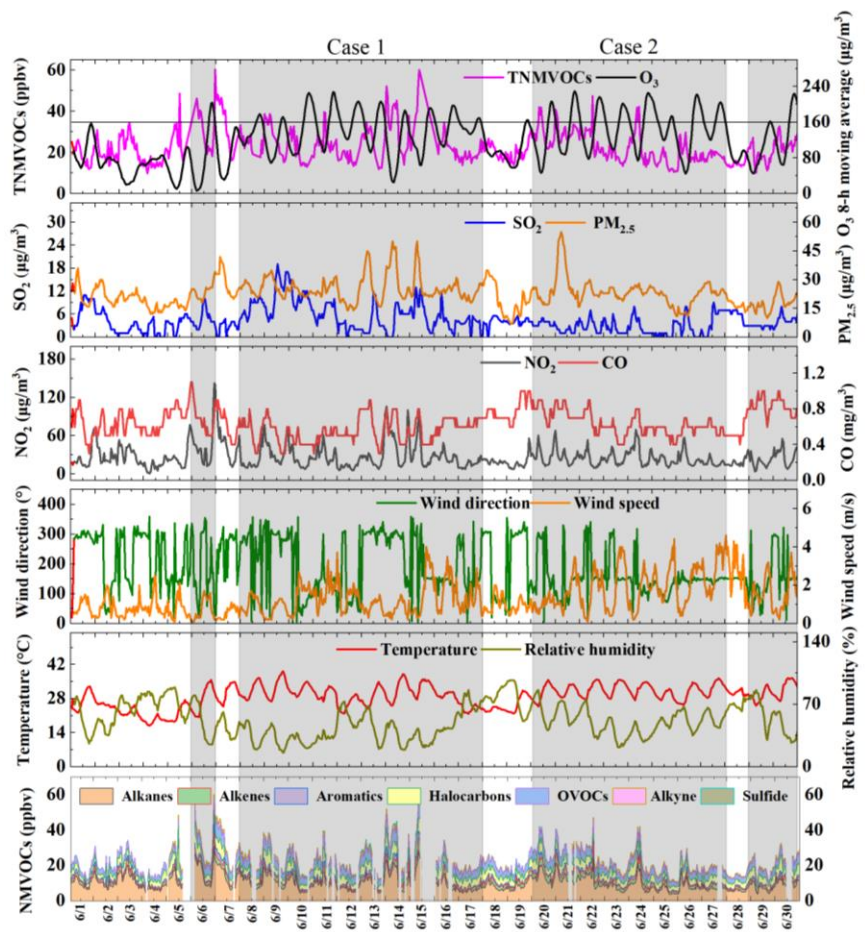


**Figure 1.** Hourly concentrations of TNMVOCs, O<sub>3</sub> 8-h moving average, SO<sub>2</sub>, PM<sub>2.5</sub>, NO<sub>2</sub>, CO, meteorological parameters (WD, WS, T, and RH), and NMVOCs during the sampling period (gray regions represent O<sub>3</sub> pollution processes).

The means and standard deviations of NMVOCs groups during different processes were listed in Table 1. During the entire period, the concentration of TNMVOCs varied from 10 to 60 ppbv, with an average mean of  $23.0 \pm 8.0$  ppbv. A similar level of NMVOCs concentration was observed between Case 1 ( $24.0 \pm 9.0$  ppbv) and Case 2 ( $23.0 \pm 7.0$  ppbv). The TNMVOCs concentrations on clean days were relatively low ( $21 \pm 7$  ppbv). Furthermore, nearly all NMVOCs groups in O<sub>3</sub> pollution events were higher than those on clean days.

As for the entire sampling period, alkanes ( $10.0 \pm 4.4$  ppbv), OVOCs ( $4.5 \pm 1.3$  ppbv), and halocarbons ( $4.3 \pm 1.9$  ppbv) were the most abundant NMVOCs groups, accounting for 44, 20 and 19% of the TNMVOCs, respectively, followed by alkenes (9%), aromatics (5%), alkenes (5%), OVOCs (7%), alkyne (7%) and sulfide (1%). During the two O<sub>3</sub> pollution events, alkanes being the highest NMVOCs group contributed 41% (Case 1), and 43% (Case 2) to the TNMVOCs, respectively. Alkanes were the most abundant NMVOCs during the observation period, in part due to the presence of alkanes emission sources around the observation site (e.g., civilian combustion and motor vehicle emissions) and the low photochemical reactivity of alkanes (Mozaffar et al., 2020). Even on clean days, alkanes ( $9.6 \pm 3.9$  ppbv) were also the highest group (46%), and halocarbons

275 (19%) and OVOCs (19%) were another two major groups.

276 **Table 1.** Concentrations of NMVOCs during different processes in Zhengzhou, ppbv.

Species	Entire period (n = 652)		Case 1 Jun. 8 - 17 (n = 201)		Case 2 Jun. 20 - 27 (n = 184)		Clean days (n = 224)	
	Range	Average $\pm$ SD	Range	Average $\pm$ SD	Range	Average $\pm$ SD	Range	Average $\pm$ SD
Alkanes	3.6 - 30.7	10.0 $\pm$ 4.4	4.2 - 28.3	10.0 $\pm$ 4.6	3.6 - 24.6	9.6 $\pm$ 4.1	4.6 - 22.2	9.6 $\pm$ 3.9
Alkenes	0.4 - 10.7	2.0 $\pm$ 1.2	0.6 - 10.7	1.9 $\pm$ 1.2	0.6 - 10.7	2.5 $\pm$ 1.4	0.4 - 4.0	1.7 $\pm$ 0.7
Aromatics	0.3 - 5.0	1.1 $\pm$ 0.7	0.4 - 4	1.2 $\pm$ 0.8	0.3 - 3.1	1.1 $\pm$ 0.6	0.3 - 4.4	1.1 $\pm$ 0.6
Halocarbons	1.8 - 31.1	4.3 $\pm$ 1.9	2.0 - 10.6	4.5 $\pm$ 1.8	2.2 - 8.8	4.2 $\pm$ 1.4	1.8 - 31.1	3.9 $\pm$ 2.2
OVOCs	1.8 - 9.7	4.5 $\pm$ 1.3	3.4 - 9.7	5.3 $\pm$ 1.2	2.0 - 8.1	4.4 $\pm$ 1.1	1.8 - 8.6	3.9 $\pm$ 1.2
Sulfide	0.0 - 1.5	0.1 $\pm$ 0.2	0.0 - 1.5	0.2 $\pm$ 0.3	0.0 - 0.5	0.1 $\pm$ 0.1	0.0 - 1.0	0.1 $\pm$ 0.1
Alkyne	0.1 - 3.7	1.1 $\pm$ 0.6	0.2 - 3.2	1.1 $\pm$ 0.6	0.2 - 3.2	1.0 $\pm$ 0.5	0.1 - 3.7	1.0 $\pm$ 0.7
TNMVOCs	9.9 - 60.3	22.8 $\pm$ 8.3	0 - 60.0	24.1 $\pm$ 8.9	10.5 - 47.3	22.5 $\pm$ 7.4	9.9 - 48.5	20.8 $\pm$ 7.2

277 n: Total sampling numbers for each period

278 Figure 2 illustrates the fifteen NMVOCs with the highest average mixing ratio during two O<sub>3</sub> pollution events  
279 and clean days. Ethane, propane, n-butane, isopentane, isobutane, n-hexane, and n-pentane were the most  
280 abundant of the alkanes during each of the entire observation period. Ethane is a major component of natural  
281 gas (NG) (Thijssse et al., 1999), propane, n-butane, and isobutane are important tracers of liquefied petroleum  
282 gas (LPG) (Tsai et al., 2006; An et al., 2014). N-hexane is mainly from solvent emissions. Ethylene, propylene,  
283 and isoprene were the most abundant of the alkenes. Ethylene and propylene mainly come from biomass  
284 burning (Andreae and Merlet, 2001). Isoprene mainly comes from plants (Brown et al., 2007). Acetylene also  
285 had a high level, which is the tracer of incomplete combustion (Blake and Rowland, 1995). Benzene and  
286 toluene were the most abundant of the aromatics, which are mainly from solvent emissions, vehicular exhaust,  
287 and industry processes (Seila et al., 2001; Mo et al., 2015). Dichloromethane was the most abundant species  
288 of the halohydrocarbons, which is an important species in solvent usage (Huang et al., 2014). The acetone was  
289 the most abundant species in OVOCs, which has complex atmospheric sources and is mainly attributed to  
290 vehicular emission and secondary formation (Guo et al., 2013; Watson et al., 2001). The concentration of  
291 acetone in the two pollution processes was significantly higher than that in the clean day as also reported by  
292 others (Guo et al., 2013), indicating that the pollution process had a strong photochemical reaction e.g., photo-  
293 oxidation of i-butene to acetone (Guo et al., 2013). Therefore, vehicle exhaust, solvent use, combustion,  
294 biogenic emission, and industrial processes are important sources of NMVOCs at observation sites, as also  
295 illustrated in the following PMF source apportionment (in section 3.2.2).

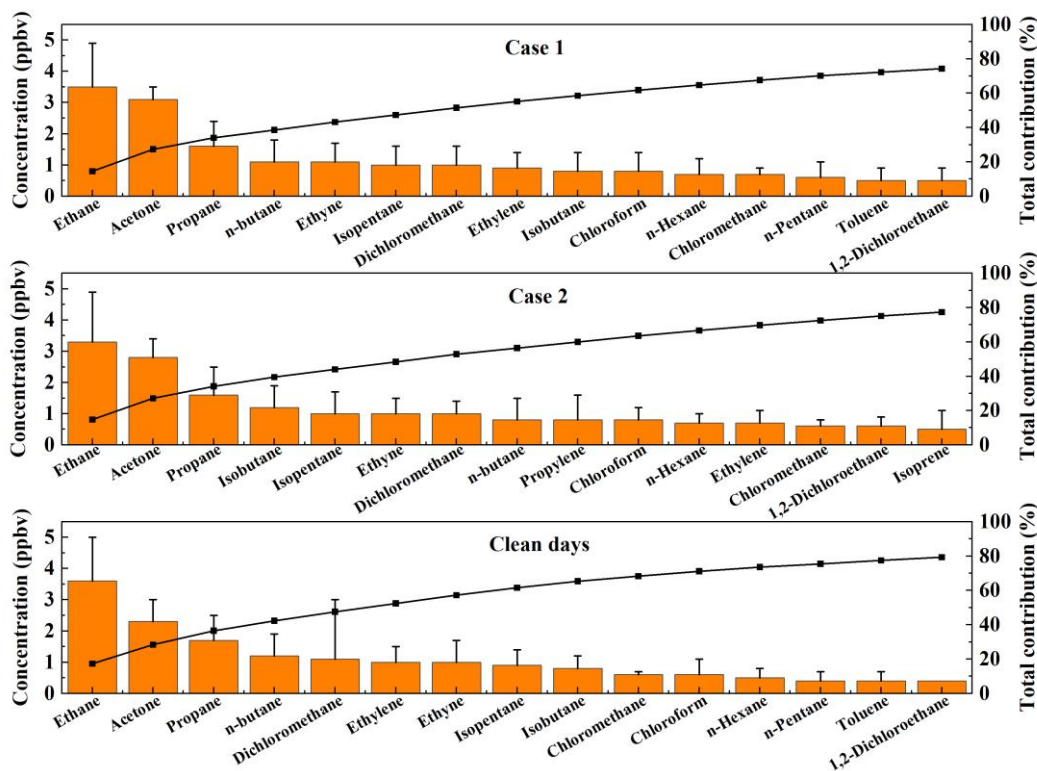


**Figure 2.** Comparisons of the fifteen NMVOCs with the highest average mixing ratio during different processes, ppbv. Error bars are standard deviations.

### 3.1.2 Diurnal variations of NMVOCs, O<sub>3</sub>, and NO<sub>x</sub>

The concentration characteristics of pollutants in the atmosphere are affected by the atmospheric boundary layer variation pattern, photochemical reaction intensity, and emission of pollution sources (Wang et al., 2023a). A selection of NMVOCs, O<sub>3</sub>, and NO<sub>x</sub> were selected, and their daily changes were analyzed, as shown in Fig. S4. The diurnal variation of O<sub>3</sub> concentration shows unimodal characteristics. During the day, with the increase in temperature and light intensity, the concentration of O<sub>3</sub> gradually increased and reached a peak at about 14:00, and then the concentration gradually decreased. Higher O<sub>3</sub> production during the day indicates a strong photochemical reactivity. The diurnal variation of ethane, propane, isobutane, n-butane, isopentane, n-pentane, ethylene, propylene, acetylene, benzene, and toluene were similar, showing low concentrations in the daytime and high concentrations in the evening. This is associated with a higher boundary layer and strong photochemical reactivity during the day (Tang et al., 2007). The elevated boundary layer is conducive to the dispersion of NMVOCs and other pollutants (Bon et al., 2011; Chen et al., 2022a), while the strong photochemical reaction will consume NMVOCs (Xia et al., 2014; Zhang et al., 2018). In addition, the peak concentrations of these NMVOCs were observed in the morning and evening (7:00-8:00 and 23:00-24:00), showing a consistent daily pattern with NO<sub>x</sub>. This suggests that the emissions of these NMVOCs are significantly influenced by motor vehicle emissions and fuel combustion. Higher NMVOCs and NO<sub>x</sub> concentrations at night may be caused by heavy traffic emissions for traditional nighttime activities in the city.

316 Isoprene is a typical tracer of plant emissions, which are highly dependent on temperature and solar radiation  
317 (Pacifico et al., 2009). Therefore, the concentration of isoprene increases significantly during the day (7:00-  
318 20:00) and decreases significantly at night. It is worth noting that the concentration of isoprene showed a  
319 bimodal characteristic. Two peaks occur at 10:00 AM and 15:00 PM (local standard time). Previous studies  
320 have shown that the rate at which plants emit isoprene decreases when temperatures exceed 40 °C (Guenther  
321 et al., 1993). Therefore, the drop in isoprene concentrations seen at noon may be due to excessive temperatures  
322 affecting biogenic emissions. Acetone comes from a wide range of sources, mainly from vehicle emissions,  
323 industrial production, and secondary formation (Sha et al., 2021). Acetone remained in high concentration  
324 throughout the day, and there was no obvious diurnal variation, suggesting that there might be primary acetone  
325 sources near the site, which concealed the acetone peak at the daytime produced by photochemical reaction  
326 (Guo et al., 2013). Dichloromethane mainly comes from solvent use, and its high concentration was mainly  
327 concentrated at night (23:00-5:00), which might be related to the longer atmospheric lifetime of  
328 dichloromethane and the lower boundary layer height at night (Li et al., 2018; Chen et al., 2022a).

## 329 3.2 Sources of NMVOCs

### 330 3.2.1 Diagnostic ratios

331 Ratios of specific NMVOCs can be used to assess the initial emission source of NMVOCs or the degree of  
332 photochemical reaction (Miller et al., 2012; An et al., 2014). The ratios of isopentane/n-pentane,  
333 toluene/benzene (T/B), and m-p-xylene/ethylbenzene (E/X) are discussed in this study (Fig. 3).

334 In Case 1, Case 2, and clean days, the Pearson coefficients of isopentane and n-pentane were 0.7, 0.94, and  
335 0.6, respectively, indicating a strong correlation that the two substances had a common emission source.  
336 Isopentane/n-pentane ratios of 0.8-0.9, 2.2-3.8, 1.5-3.0 and 1.8-4.6 (Fig. 3a), indicate that isopentane and n-  
337 pentane come from natural NG, vehicle emissions, liquid gasoline, and fuel evaporation, respectively (An et  
338 al., 2014; Watson et al., 2001). In this study, the ratios of Case 1, Case 2, and clean days were 0.7, 2.5, and  
339 1.1, respectively. It suggests that isopentane and n-pentane may come from NG emissions, vehicular exhaust,  
340 and liquid gasoline, respectively.

341 The T/B ratio can be used to distinguish between coal and biomass combustion (0.2-0.6), motor vehicle  
342 emissions (~2.0) (Liu et al., 2008), industrial processes (3.0-6.9) (Zhang et al., 2016) and fuel evaporation  
343 (~4.1) (Dai et al., 2013). In this study, the T/B ratio of the two O<sub>3</sub> pollution events was 1.7 and 1.4 (Fig. 3b),  
344 respectively, indicating that combustion and vehicle emissions were the main sources of benzene and toluene  
345 emissions (Hong et al., 2019).

346 Since m/p-xylene and ethylbenzene share a common source, but differ from the OH radical reaction rate



constant, E/X can be used to determine the photochemical age of air masses and the transport path (Miller et al., 2012; Yurdakul et al., 2018). During the pollution events and clean days, m, p-xylene, and ethylbenzene showed a strong positive correlation ( $r = 0.9$ ) (Fig. 3c), indicating that m/p-xylene and ethylbenzene came from a common emission source. Previous studies have shown that NMVOCs are transported from inner urban areas when the E/X ratio is 0.3-0.4, and NMVOCs are transported from distant sources when the ratio is significantly higher than 0.3 (Monod et al., 2001). In this study, the E/X ratios of the two pollution events and clean days were 0.5, indicating that the air mass measured at the observation point was affected by air mass transport. We have analyzed the relationship between ethylbenzene, m/p-Xylene, E/X, and wind direction and speed. As shown in Fig. S5, the concentrations of ethylbenzene and m/p-Xylene are mainly influenced by winds coming from the northwest, and their concentrations tend to increase with stronger wind speeds. Similarly, E/X also exhibits similar patterns of variation. This further indicates that the regional transport of ethylbenzene and m/p-Xylene from distant sources.

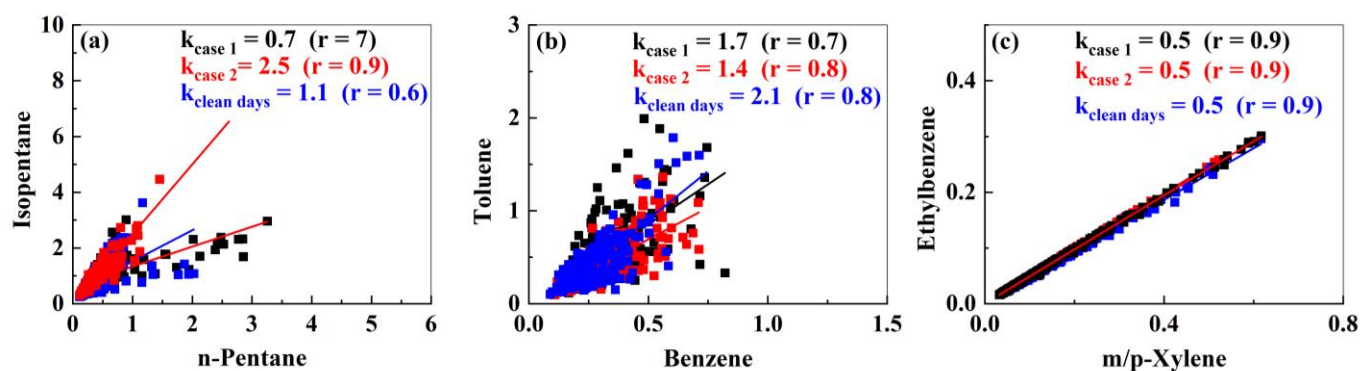


**Figure 3.** Correlations ( $k = \text{slope}$ ) between compounds with different observation periods.

### 3.2.2 Source apportionment

In this study, EPA PMF5.0 was used to analyze the source profile and species percentage of each source during the observation period to determine the relative contribution of each potential source, as shown in Fig. 4. Seven factors were determined by the model, namely combustion, industrial production, biogenic emission, vehicular exhaust, LPG/NG, solvent use 1, and solvent use 2. Detailed analysis is followed.

Factor 1 was characterized by high percentages of acetylene (76%), ethane, propane, ethylene benzene, and toluene. Acetylene is a typical tracer of coal burning (Barletta et al., 2005). Ethane, propane, and ethylene are typically tracers of incomplete combustion (Guo et al., 2011; Ling et al., 2011). Therefore, Factor 1 was classified as combustion. The CPF plots indicate that the contributing direction was northwest at about 2 m/s (Fig. S6a).

Factor 2 was rich in C4-C6 alkanes, aromatics, (toluene, ethylbenzene, m/p-Xylene, o-xylene, and 1,2,4-trimethylbenzene, and halocarbons (1, 2-dichloroethane and 1, 2-dichloropropane). Previous studies have



373 shown that these species were all related to industrial production. Therefore, Factor 2 was classified as  
374 industrial production. The CPF plots indicated that a local source under a low wind speed of  $< 1$  m/s was the  
375 dominant source (Fig. S6b).

376 Factor 3 was characterized by high percentages (83%) of isoprene, a typical tracer of biogenic emission  
377 (Brown et al., 2007). The high temperature and strong radiation in summer are more conducive to the biogenic  
378 emission of isoprene (Liu et al., 2016). Therefore, Factor 3 was classified as a biogenic emission. The CPF  
379 plots indicated that the southwest was the dominant source direction under wind speeds below 2 m/s (Fig.  
380 S6c).

381 Factor 4 was characterized by high percentages of C2-C6 alkanes (such as ethane, propane, isobutane, n-  
382 butane, isopentane, n-pentane, 2, 2-dimethylbutane, and 2, 3-dimethylbutane), benzene, toluene, ethylbenzene,  
383 and m/p-xylene), which are related to vehicular emission (Jorquera and Rappenglück, 2004; Song et al., 2007;  
384 Chen et al., 2014). Therefore, Factor 4 was classified as vehicular exhaust. The CPF plots indicated that a local  
385 source under a low wind speed was the dominant source, which might be related to the large amount of traffic  
386 on the main roads in the southern and western directions direction (Fig. S6d).

387 Factor 5 was characterized by high percentages of ethane, propane, isobutane, and propylene, which are the  
388 main components of LPG/NG (Shao et al., 2016; Song et al., 2007; Na et al., 2001). Therefore, Factor 5 was  
389 classified as LPG/NG source. The CPF plots showed the dominant source directions of this factor were east  
390 at 1-2 m/s (Fig. S6e).

391 Factor 6 was characterized by high percentages of chloromethane, dichloromethane, tetrachloromethane, 1,2-  
392 dichloroethane, 1,2-dichloropropane, and ethyl acetate, which are typical solvents for industrial applications  
393 (Li et al., 2020; Huang et al., 2014). Therefore, Factor 6 was assigned to solvent usage 1. The CPF plots of  
394 this factor indicated that the northeast and southeast were the dominant directions (Fig. S6f).

395 The Factor 7 was dominated by methylcyclopentane, cyclohexane, TEXs (Toluene, Ethylbenzene, m/p-Xylene,  
396 and o-Xylene) , 1,2-Dichloroethane 、 1,2-Dichloropropane, and Ethyl acetate. Methylcyclopentane and  
397 cyclohexane were commonly used as solvents in industrial processes (Lyu et al., 2016; Yuan et al., 2013).  
398 TEX is the main component of organic solvents (Guo et al., 2011; Watson et al., 2001). Therefore, Factor 7  
399 was assigned to solvent usage 2. The CPF plots of this factor indicate that the high CPF values were found  
400 near the center when the wind speed was low ( $\leq 1$  m/s). This finding indicates that local emissions was the  
401 dominant source (Fig. S6g).

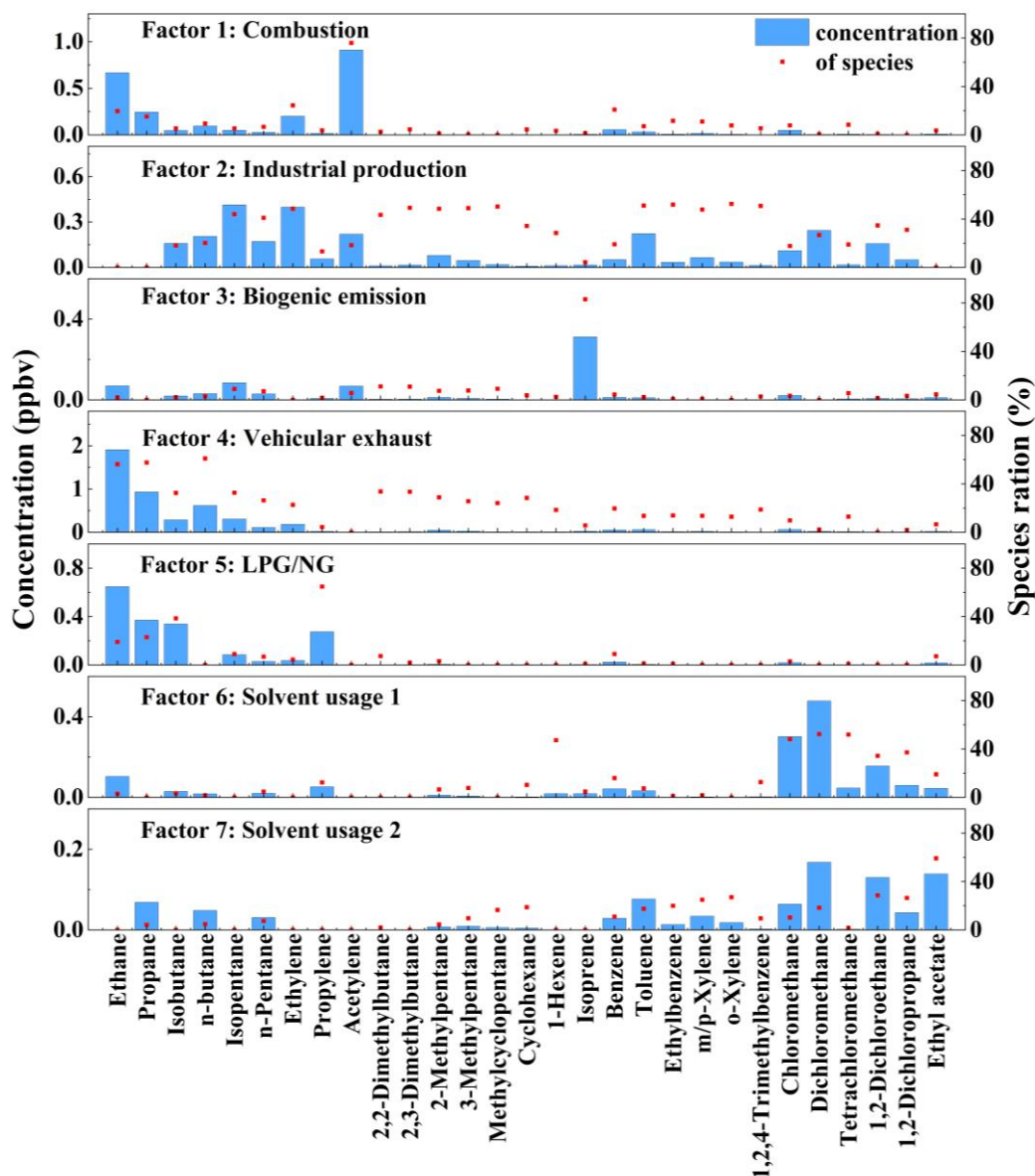


**Figure 4.** Source profiles and contributions of NMVOCs during the observation period.

Figure 5 shows the proportion of each NMVOCs source during the observation process. In the entire observation period, vehicular exhaust is the main contributor, accounting for 28%, followed by solvent usage (27%) and industrial production (22%). Other sources including LPG/NG (9%), combustion sources (8%), and biogenic emission (6%) contributed little. In Case 1, vehicular exhaust (30%) was the largest contributor, followed by solvent usage (27%) and industrial production (23%). Compared with the Case 1 event, the contribution of solvent usage and industrial production in the Case 2 event did not change much, and the contribution of LPG/NG increased by 14%, which became an important source. On clean days, vehicular exhaust (35%), solvent usage (25%), and industrial production (21%) were the most significant contributors. Compared with clean days, the contribution of solvent usage, industrial production, biogenic emission, and LPN/NG in both pollution events increased, while the contribution of combustion sources and vehicular exhaust decreased. In summary, vehicular exhaust, solvent usage, and industrial production were major contributors to both O<sub>3</sub> pollution events and clean days.

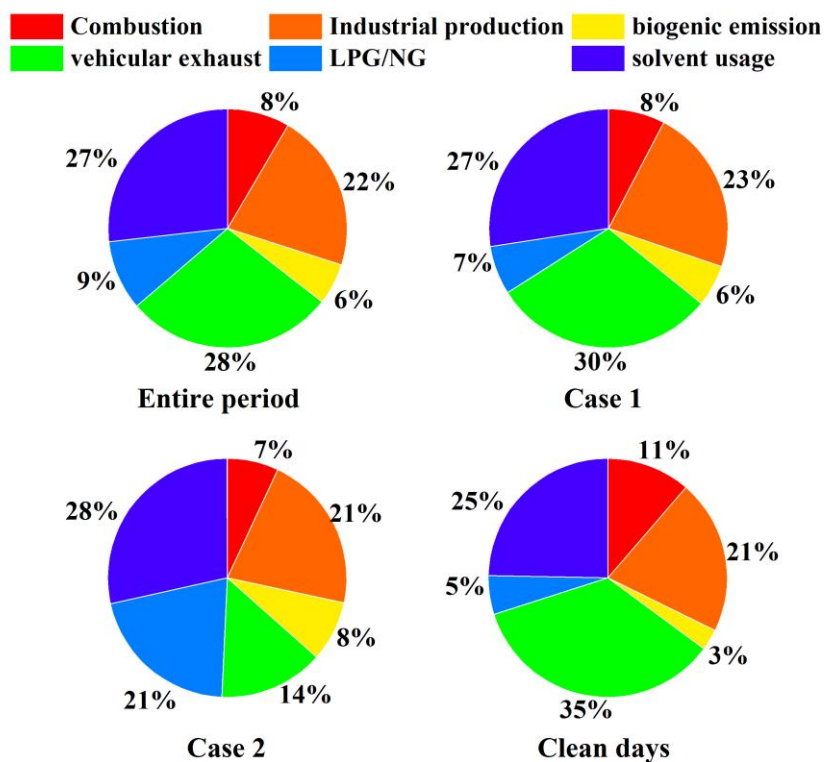


**Figure 5.** Source contributions to NMVOCs concentration during different periods.

In summary, the observation sites are significantly influenced by vehicular exhaust, solvent usage, and industrial production. The results of this study show similarities in the source apportionment of NMVOCs in Zhengzhou during the summers of 2018 to 2021 (Yu et al., 2022; Guo et al., 2024). Yu et al. (2022) found that vehicular exhaust and industrial production contributed the most to NMVOCs emissions in Zhengzhou from 2018 to 2020, with the main sources of summer NMVOCs being vehicular exhaust, solvent usage, and industrial production. In contrast to the NMVOCs source apportionment results of Li et al. (2021), for the O<sub>3</sub> pollution process in Zhengzhou in May 2018, the difference lies in the higher impact of solvent usage compared to vehicular exhaust and industrial production. This is mainly attributed to the fact that Li et al. (2021)'s observation site was located within Zhengzhou University, making them more susceptible to the influence of chemical reagent use. In comparison to the source apportionment of NMVOCs in Zhengzhou during winter (Zhang et al., 2021), combustion also becomes an important contributor during winter, attributed to the increased heating demand, while the contribution from solvent usage is relatively lower due to the cold temperatures. In comparison with other cities (Table S2), vehicular exhaust in Zhengzhou contributes the most, higher than in cities such as Qingdao (Wu et al., 2023), Xuchang (Qin et al., 2021), Guangzhou (Meng et al., 2022), Nanjing (Fan et al., 2021), Shijiazhuang (Guan et al., 2020), and Weinan (Hui et al., 2020), but lower than in Changzhou (Liu et al., 2023) and on par with Beijing (Liu et al., 2020). Solvent usage in Zhengzhou contributes more than in Qingdao (Wu et al., 2023), Xuchang (Qin et al., 2021), Nanjing (Fan et al., 2021), Shijiazhuang (Guan et al., 2020), Weinan (Hui et al., 2020), Changzhou (Liu et al., 2023), and Beijing (Liu et

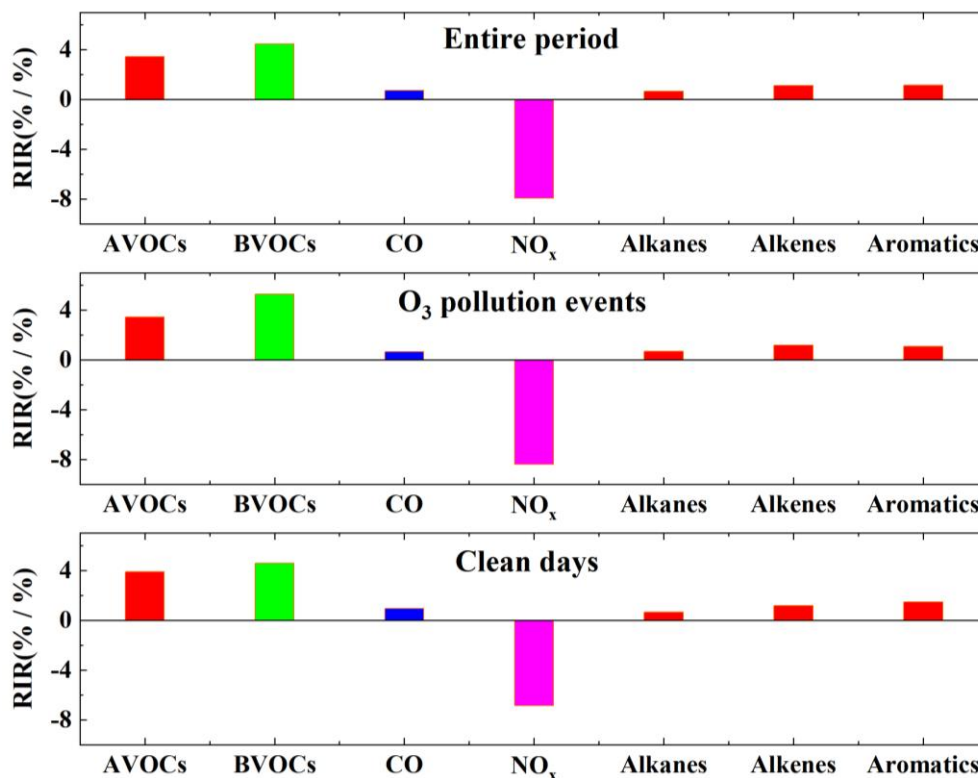
al., 2020), but less than in Guangzhou (Meng et al., 2022). Industrial production in Zhengzhou contributes more than in Xuchang (Qin et al., 2021), Guangzhou (Meng et al., 2022), Nanjing (Fan et al., 2021), Weinan (Hui et al., 2020), and Changzhou (Liu et al., 2023), but less than in Shijiazhuang (Guan et al., 2020).

### 3.3 Contribution to O<sub>3</sub> formation

#### 3.3.1 O<sub>3</sub> sensitivity analysis

In this study, the RIR of AVOCs, BVOCs, CO, NO<sub>x</sub>, alkanes, alkenes, and aromatics were calculated (Fig. 6). The RIR values of NMVOCs were all positive during the entire period, indicating that O<sub>3</sub> generation is most sensitive to NMVOCs reduction. In comparison, the RIR value of NO<sub>x</sub> was negative, indicating that reduction of NO<sub>x</sub> would cause the increasing of the O<sub>3</sub> concentrations. Among AVOCs, aromatics had the highest RIR value, followed by alkanes and aromatics. For both O<sub>3</sub> pollution events and clean days, the RIR value of NO<sub>x</sub> was negative, and the RIR of NMVOCs and CO were positive. In pollution events, apart from BHC, the absolute values of RIR for each group and species are lower than those in clean days, indicating that the sensitivity of O<sub>3</sub> to NMVOCs, NO<sub>x</sub>, and CO on clean days was higher than that in the O<sub>3</sub> pollution events. Compared to clean days, the RIR value of AVOCs decreased by 11%, with Aromatics showing the largest decrease (26%), while Alkanes and Alkenes increased by 7% and 3% respectively. In pollution events, CO and NO<sub>x</sub> were reduced by 29% and 22%, respectively.

Isoprene was the sole BVOC considered in this study. Isoprene is an important tracer to indicate biogenic emissions (Xie et al., 2021; Li et al., 2024; Qin et al., 2023). During the entire period, especially in the pollution events, the RIR of AVOCs was lower than that of BVOCs, indicating that O<sub>3</sub> formation was more sensitive to biogenic emissions. This may be due to increased emissions of BVOCs at higher temperatures and solar radiation conditions, as well as their high reactivity and O<sub>3</sub> formation potential. Studies in Yucheng (Zong et al., 2018), Leshan (Xie et al., 2021), and Nanjing (Fan et al., 2021; Ming et al., 2020) have shown that O<sub>3</sub> is highly sensitive to BVOCs. Studies in Zhengzhou (Wang et al., 2022), Hangzhou (Zhao et al., 2020), and Hong Kong (Wang et al., 2017) suggested that O<sub>3</sub> exhibits greater sensitivity to BVOCs than AVOCs during hot seasons. Wang et al. (2019) found in their study on O<sub>3</sub> source apportionment in Henan Province, where Zhengzhou is located, that BVOCs contribute to approximately 23.9% of the O<sub>3</sub> attributed to NMVOCs. Therefore, the contribution of BVOCs to O<sub>3</sub> is very important.



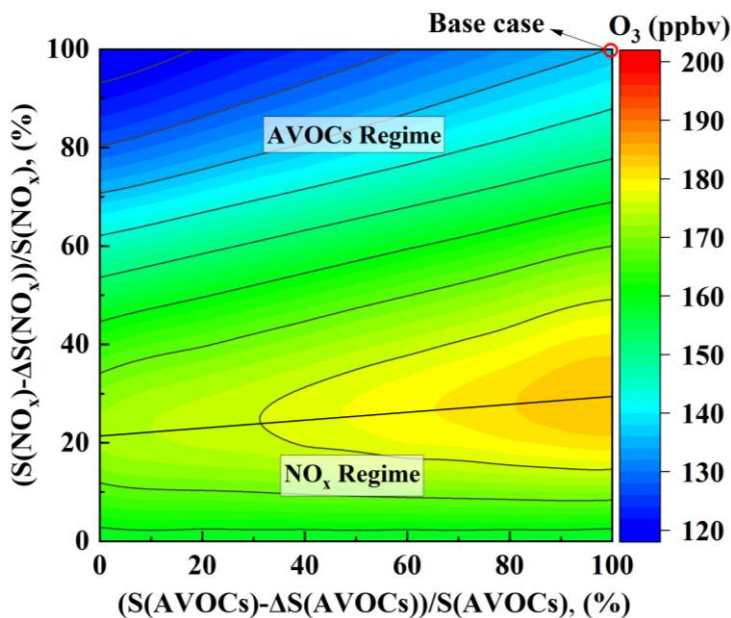
463 **Figure 6.** Average RIR values of the O<sub>3</sub> for different species/groups during different processes in Zhengzhou.

### 465 3.3.2 Empirical kinetics modeling approach (EKMA) results

466 Given the current inability to implement appropriate control measures for BVOCs, the following analysis  
 467 considers only the impact of AVOCs and NO<sub>x</sub> on O<sub>3</sub> formation. The EKMA curve drawn based on the OBM  
 468 model is shown in Fig. 7. It can be seen from the EKMA curve that O<sub>3</sub> generation presents a highly nonlinear  
 469 relationship with its precursor compounds AVOCs and NO<sub>x</sub>, and the same O<sub>3</sub> concentration can be generated  
 470 by different concentration combinations of AVOCs and NO<sub>x</sub>. In the figure, AVOCs and NO<sub>x</sub> = 100% is the  
 471 base case, and the horizontal and vertical axes represented the percentages of AVOCs and NO<sub>x</sub> relative to the  
 472 actual observed mixture ratio (100%). The straight lines in the figure are called ridgeline and is formed by the  
 473 junction of turning points of O<sub>3</sub> concentration lines (Dodge, 1977).

474 The ridge divides the graph into the upper left and the lower right parts, and there are also large differences in  
 475 O<sub>3</sub> generation between these two parts. In the lower right part, each O<sub>3</sub> concentration line and the horizontal  
 476 coordinate show a parallel relationship. If the NO<sub>x</sub> concentration is maintained unchanged, the O<sub>3</sub>  
 477 concentration does not change with the change of AVOCs concentration. When the AVOCs concentration is  
 478 unchanged, the concentration of O<sub>3</sub> decreases with the decrease of NO<sub>x</sub> concentration. Therefore, in this part  
 479 of the region, O<sub>3</sub> generation is controlled by NO<sub>x</sub>. In the upper left part, if the concentration of AVOCs is  
 480 reduced alone, the concentration of O<sub>3</sub> will decrease significantly; if only the concentration of NO<sub>x</sub> is reduced,  
 481 the concentration of O<sub>3</sub> will first rise and then decrease. In this region, O<sub>3</sub> generation is in the control region  
 482 of AVOCs. In the area near the ridge line, when NO<sub>x</sub> and AVOCs are reduced at the same time, the O<sub>3</sub>

483 concentration will decrease, and the O<sub>3</sub> generation in the cooperative control area of AVOCs and NO<sub>x</sub>.  
 484 The ridgeline slope of this EKMA curve was about 6:1, that was, the reduction of NO<sub>x</sub> and AVOCs along this  
 485 ridge was the fastest way to reduce the O<sub>3</sub> concentration. As can be seen from the figure, Zhengzhou was a  
 486 typical AVOCs control area, and O<sub>3</sub> was very sensitive to the changes of AVOCs. At the same time, Case 1,  
 487 Case 2, and clean days are all above the ridgeline and belong to the AVOCs control region (Fig. S7). Therefore,  
 488 reducing AVOCs can effectively reduce the generation of O<sub>3</sub>.



489  
 490 **Figure 7.** Isopleth diagram of modeled O<sub>3</sub> on S(AVOCs) and S(NO<sub>x</sub>) remaining percentages.

491 **3.3.3 Control strategies of O<sub>3</sub>**

492 The above analysis based on single species (NO<sub>x</sub> or AVOCs) is only used to discuss the sensitivity of O<sub>3</sub>  
 493 concentration to precursor, but such extreme control is difficult to achieve. Usually in the actual operation, the  
 494 method of simultaneously controlling NO<sub>x</sub> and AVOCs emissions is usually adopted to reduce the  
 495 concentration of O<sub>3</sub>. To establish a reasonable and effective AVOCs and NO<sub>x</sub> emission reduction plan, we  
 496 further conducted a series of simulations to calculate the O<sub>3</sub> concentration by adjusting the ratio of input  
 497 AVOCs and NO<sub>x</sub>. The following analyzes the reduction cases of O<sub>3</sub> control at 10 a.m. to 4 p.m. during the  
 498 observation period.

499 Figure 8 shows different reduction schemes. In Fig. 8, the horizontal and vertical axes corresponded to the  
 500 reduction percentages of NO<sub>x</sub> or NO<sub>x</sub> + AVOCs and the reduction percentage of O<sub>3</sub> concentration (positive  
 501 and negative values represent the increase and decrease of O<sub>3</sub> concentration compared to the base case). The  
 502 results show that O<sub>3</sub> concentration will eventually decline regardless of the reduction method, but the trend of  
 503 change varies (Fig. 8a). As can be seen from Fig. 8b, if only NO<sub>x</sub> was reduced, when the emission reduction  
 504 was less than 60%, the change in O<sub>3</sub> concentration shows an increasing trend; when the emission reduction



was greater than 60%, the change of O<sub>3</sub> concentration shows a decreasing trend. Therefore, only NO<sub>x</sub> emission reduction was not conducive to the reduction of O<sub>3</sub> concentration. When the reduction ratio of AVOCs/NO<sub>x</sub> was 1:2 and 1:1, the change in O<sub>3</sub> concentration shows a similar trend as that of NO<sub>x</sub> emission reduction only, and O<sub>3</sub> concentration increases first and then decreases. When the reduction ratio of AVOCs/NO<sub>x</sub> was 2:1, O<sub>3</sub> concentration increases to a certain extent. When the emission reduction ratio of AVOCs/NO<sub>x</sub> was 3:1 or 4:1, O<sub>3</sub> concentration continues to decline, and the decline rate of O<sub>3</sub> concentration of 4:1 was greater than 3:1. If only AVOCs emission was reduced, O<sub>3</sub> concentration shows a continuous downward trend, and the decline rate was very fast. However, combined with actual production activities, only reducing AVOCs emissions cannot be achieved, which was not conducive to policy implementation. Therefore, from the perspective of comprehensive emission reduction effect, the reduction ratio of AVOCs/NO<sub>x</sub> should be no less than 3:1, which will be conducive to the reduction of O<sub>3</sub> concentration.

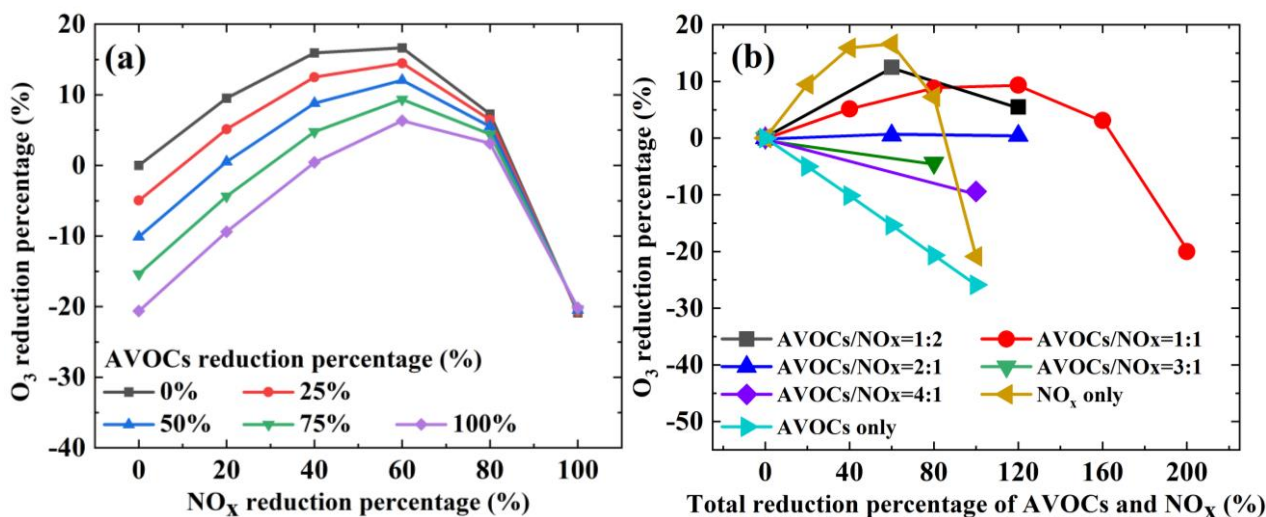


**Figure 8.** Response of the O<sub>3</sub> concentration to different AVOCs and NO<sub>x</sub> reduction percentages. Note: AVOCs/NO<sub>x</sub> was the ratio of the percentage reduction of AVOCs and NO<sub>x</sub>.

In addition, this study analyzed O<sub>3</sub> reduction schemes from 10 a.m. to 4 p.m. It can be seen from Fig. S8 that with the reduce of NO<sub>x</sub>, O<sub>3</sub> concentration elevated and then decreased. When the reduction ratio of AVOCs was fixed and the reduction ratio of NO<sub>x</sub> was less than 60%, O<sub>3</sub> concentration increases with the reduce of NO<sub>x</sub>. In this case, O<sub>3</sub> concentration increased by 30, 21, 16, 13, 13, 15, and 15% from 10 a.m. to 4 p.m. (that is, under the AVOCs scenario without reduction). When the NO<sub>x</sub> reduction ratio was greater than 60%, O<sub>3</sub> concentration decreases with the reduce of NO<sub>x</sub>. When the reduction was the greatest (that is, 100% reduction of NO<sub>x</sub> and AVOCs), O<sub>3</sub> concentration at 10 o'clock was still increased compared with the atmospheric observation concentration, increased by 14%; O<sub>3</sub> concentration at 11 a.m. to 4 p.m. decreased by 2, 15, 25, 32, 36, and 36%, respectively.

Between the range of 10 a.m. to 4 p.m. in the day, when only NO<sub>x</sub> was reduced, O<sub>3</sub> concentration elevated and

529 then decreased. When only AVOCs were reduced, O<sub>3</sub> concentration continued to decrease. When the reduction  
530 ratio of AVOCs/NO<sub>x</sub> was less than 2:1, O<sub>3</sub> concentration elevated and then decreased. When the reduction  
531 ratio of AVOCs/NO<sub>x</sub> was greater than 2:1, O<sub>3</sub> concentration continues to decrease. When AVOCs/NO<sub>x</sub> = 4:1,  
532 O<sub>3</sub> concentration decreases the most and the fastest. According to the reduction ratio of AVOCs/NO<sub>x</sub> = 4:1,  
533 the maximum reduction of O<sub>3</sub> concentration at 10 a.m. to 4 p.m. during the day were 3, 6, 10, 11, 13, and 13%,  
534 respectively.

#### 535 4 Conclusions

536 The summer O<sub>3</sub> pollution has always been an important environmental issue in Zhengzhou. This study  
537 investigated the characteristics and emission sources of O<sub>3</sub> precursors from 1<sup>st</sup> to 30<sup>th</sup> June 2023. The OBM  
538 was used to analyze the influence of precursors on the formation of O<sub>3</sub>, and the emission reduction strategy of  
539 precursors was proposed to control the concentration of O<sub>3</sub>. During the entire period, the concentration of  
540 TNMVOCs varied from 9.9 to 60.3 ppbv, with an average value of 22.9 ± 8.3 ppbv. The average  
541 concentration of TNMVOCs during O<sub>3</sub> pollution was higher than that during clean days. Alkanes (44%),  
542 OVOCs (20%), and halocarbons (19%) were the most abundant NMVOCs group. Ethane, acetone, and  
543 propane were always the most abundant species. The average concentrations of NO<sub>2</sub> in pollution events were  
544 higher than those in clean days, while the average concentrations of NO were lower than those in clean days.  
545 Therefore, the increasing concentration of O<sub>3</sub> precursors is one of the reasons for the formation of O<sub>3</sub> pollution.  
546 At the same time, the unfavorable meteorological conditions of high temperature and low RH in the  
547 observation process are also important factors in the formation of O<sub>3</sub> pollution. Further analysis of the source  
548 of these precursors found that Vehicular exhaust (28%), solvent usage (27%), and industrial production (22%)  
549 were the main emission sources of NMVOCs. The increase of solvent usage, biogenic emission and LPN/NG  
550 contribution is an important cause of O<sub>3</sub> pollution. Sensitivity analysis of O<sub>3</sub> to precursors found that  
551 NMVOCs had the highest RIR value, while NO<sub>x</sub> had a negative RIR value. Alkenes have the highest RIR  
552 value among AVOCs. It should be noted that the RIR value of BVOCs was greater than that of AVOCs. The  
553 local O<sub>3</sub> formations were in the AVOC-limited regime, which means reducing the concentration of AVOCs  
554 was an effective way to reduce O<sub>3</sub> concentration. Meanwhile, we suggest that the minimum reduction ratio of  
555 AVOCs/NO<sub>x</sub> should be no less than 3:1 to reduce O<sub>3</sub> production.

556  
557 **Data availability.** Data can be obtained upon request from the authors.

558  
559 **Authorship contributions.** DZ performed chemical modelling analyses of OBM-MCM and wrote the paper.

560 XL collected the data and contributed to the data analysis. RZ designed and revised the paper. QX, FS, and  
561 SW contributed to discussions of results. MY and YX provided part of the data in Zhengzhou.

562  
563 **Competing interests.** The contact author has declared that neither they nor their co-authors have any  
564 competing interests.

565  
566 **Financial support.** This work was supported by National Key Research and Development Program of China  
567 (No. 2017YFC0212403).

## 568 **References**

569 An, J., Zhu, B., Wang, H., Li, Y., Lin, X., and Yang, H.: Characteristics and source apportionment of VOCs  
570 measured in an industrial area of Nanjing, Yangtze River Delta, China, *Atmos. Environ.*, **97**, 206-214,  
571 <https://doi.org/10.1016/j.atmosenv.2014.08.021>, 2014.

572 Andreae, M. O., and Merlet, P.: Emission of trace gases and aerosols from biomass burning, *Global*  
573 *Biogeochem. Cy.*, **15**, 955-966, <https://doi.org/10.1029/2000GB001382>, 2001.

574 Barletta, B., Meinardi, S., Sherwood Rowland, F., Chan, C.-Y., Wang, X., Zou, S., Yin Chan, L., and Blake,  
575 D. R.: Volatile organic compounds in 43 Chinese cities, *Atmos. Environ.*, **39**, 5979-5990,  
576 <https://doi.org/10.1016/j.atmosenv.2005.06.029>, 2005.

577 Billionnet, C., Gay, E., Kirchner, S., Leynaert, B., and Annesi-Maesano, I.: Quantitative assessments of indoor  
578 air pollution and respiratory health in a population-based sample of French dwellings, *Environ. Res.*, **111**,  
579 425-434, <https://doi.org/10.1016/j.envres.2011.02.008>, 2011.

580 Blake, D. R., and Rowland, F. S.: Urban Leakage of Liquefied Petroleum Gas and Its Impact on Mexico City  
581 Air Quality, *Science*, **269**, 953-956, <https://doi.org/10.1126/science.269.5226.953>, 1995.

582 Bon, D. M., Ulbrich, I. M., de Gouw, J. A., Warneke, C., Kuster, W. C., Alexander, M. L., Baker, A., Beyersdorf,  
583 A. J., Blake, D., Fall, R., Jimenez, J. L., Herndon, S. C., Huey, L. G., Knighton, W. B., Ortega, J.,  
584 Springston, S., and Vargas, O.: Measurements of volatile organic compounds at a suburban ground site  
585 (T1) in Mexico City during the MILAGRO 2006 campaign: measurement comparison, emission ratios,  
586 and source attribution, *Atmos. Chem. Phys.*, **11**, 2399-2421, <https://doi.org/10.5194/acp-11-2399-2011>,  
587 2011.

588 Brown, S. G., Frankel, A., and Hafner, H. R.: Source apportionment of VOCs in the Los Angeles area using  
589 Positive Matrix Factorization, *Atmos. Environ.*, **41**, 227-237,  
590 <https://doi.org/10.1016/j.atmosenv.2006.08.021>, 2007.

- 591 Callén, M. S., Iturmendi, A., and López, J. M.: Source apportionment of atmospheric PM<sub>2.5</sub>-bound polycyclic  
592 aromatic hydrocarbons by a PMF receptor model. Assessment of potential risk for human health, *Environ.*  
593 *Pollut.*, 195, 167-177, <https://doi.org/10.1016/j.envpol.2014.08.025>, 2014.
- 594 Cardelino, C. A., and Chameides, W. L.: An observation-based model for analyzing ozone precursor  
595 relationships in the urban atmosphere, *J. Air. Waste. Manage.*, 45, 161-180,  
596 <https://doi.org/10.1080/10473289.1995.10467356>, 1995.
- 597 Cardelino, C. A., and Chameides, W. L.: The application of data from photochemical assessment monitoring  
598 stations to the observation-based model, *Atmos. Environ.*, 34, 2325-2332, <https://doi.org/10.1016/S1352->  
599 [2310\(99\)00469-0](https://doi.org/10.1016/S1352-2310(99)00469-0), 2000.
- 600 Carslaw, D. C., and Ropkins, K.: openair — An R package for air quality data analysis, *Environ. Modell.*  
601 *Softw.*, 27-28, 52-61, <https://doi.org/10.1016/j.envsoft.2011.09.008>, 2012.
- 602 Chameides, W. L., Fehsenfeld, F., Rodgers, M. O., Cardelino, C., Martinez, J., Parrish, D., Lonneman, W.,  
603 Lawson, D. R., Rasmussen, R. A., Zimmerman, P., Greenberg, J., Middleton, P., and Wang, T.: Ozone  
604 precursor relationships in the ambient atmosphere, *J. Geophys. Res-Atmos.*, 97, 6037-6055,  
605 <https://doi.org/10.1029/91jd03014>, 1992.
- 606 Chen, D., Xu, Y., Xu, J., Lian, M., Zhang, W., Wu, W., Wu, M., and Zhao, J.: The Vertical Distribution of  
607 VOCs and Their Impact on the Environment: A Review, *Atmosphere*, 13, 1940,  
608 <https://doi.org/10.3390/atmos13121940>, 2022a.
- 609 Chen, D., Zhou, L., Wang, C., Liu, H., Qiu, Y., Shi, G., Song, D., Tan, Q., and Yang, F.: Characteristics of  
610 ambient volatile organic compounds during spring O<sub>3</sub> pollution episode in Chengdu, China, *J. Environ.*  
611 *Sci.*, 114, 115-125, <https://doi.org/10.1016/j.jes.2021.08.014>, 2022b.
- 612 Chen, L., Zhu, J., Liao, H., Yang, Y., and Yue, X.: Meteorological influences on PM<sub>2.5</sub> and O<sub>3</sub> trends and  
613 associated health burden since China's clean air actions, *Sci. Total. Environ.*, 744, 140837,  
614 <https://doi.org/10.1016/j.scitotenv.2020.140837>, 2020.
- 615 Chen, W. T., Shao, M., Lu, S. H., Wang, M., Zeng, L. M., Yuan, B., and Liu, Y.: Understanding primary and  
616 secondary sources of ambient carbonyl compounds in Beijing using the PMF model, *Atmos. Chem. Phys.*,  
617 14, 3047-3062, <https://doi.org/10.5194/acp-14-3047-2014>, 2014.
- 618 Chu, W., Li, H., Ji, Y., Zhang, X., Xue, L., Gao, J., and An, C.: Research on ozone formation sensitivity based  
619 on observational methods: Development history, methodology, and application and prospects in China, *J.*  
620 *Environ. Sci.*, 138, 543-560, <https://doi.org/10.1016/j.jes.2023.02.052>, 2023.
- 621 Dai, P., Ge, Y., Lin, Y., Su, S., and Liang, B.: Investigation on characteristics of exhaust and evaporative

- emissions from passenger cars fueled with gasoline/methanol blends, *Fuel*, 113, 10-16, <https://doi.org/10.1016/j.fuel.2013.05.038>, 2013.
- Dodge, M. C.: Combined use of modeling techniques and smog chamber data to derive ozone-precursor relationships, *Proceedings of the International Conference on Photochemical Oxidant Pollution and Its Control*, 2, 881-889, 1977.
- Fan, M., Zhang, Y., Lin, Y., Li, L., Xie, F., Hu, J., Mozaffar, A., and Cao, F.: Source apportionments of atmospheric volatile organic compounds in Nanjing, China during high ozone pollution season, *Chemosphere*, 263, <https://doi.org/10.1016/j.chemosphere.2020.128025>, 2021.
- Goldberg, D. L., Vinciguerra, T. P., Anderson, D. C., Hembeck, L., Canty, T. P., Ehrman, S. H., Martins, D. K., Stauffer, R. M., Thompson, A. M., Salawitch, R. J., and Dickerson, R. R.: CAMx ozone source attribution in the eastern United States using guidance from observations during DISCOVER - AQ Maryland, *Geophys. Res. Lett.*, 43, 2249-2258, <https://doi.org/10.1002/2015gl067332>, 2016.
- Goldstein, A. H., and Galbally, I. E.: Known and unexplored organic constituents in the earth's atmosphere, *Environ. Sci. Technol.*, 41, 1514-1521, <https://doi.org/10.1021/es072476p>, 2007.
- Guan, Y., Wang, L., Wang, S., Zhang, Y., Xiao, J., Wang, X., Duan, E., and Hou, L. a.: Temporal variations and source apportionment of volatile organic compounds at an urban site in Shijiazhuang, China, *J. Environ. Sci.*, 97, 25-34, <https://doi.org/10.1016/j.jes.2020.04.022>, 2020.
- Guenther, A. B., Zimmerman, P. R., Harley, P. C., Monson, R. K., and Fall, R.: Isoprene and monoterpene emission rate variability: Model evaluations and sensitivity analyses, *J. Geophys. Res-Atmos.*, 98, 12609-12617, <https://doi.org/https://doi.org/10.1029/93JD00527>, 1993.
- Guo, H., Cheng, H. R., Ling, Z. H., Louie, P. K., and Ayoko, G. A.: Which emission sources are responsible for the volatile organic compounds in the atmosphere of Pearl River Delta?, *J. Hazard. Mater.*, 188, 116-124, <https://doi.org/10.1016/j.jhazmat.2011.01.081>, 2011.
- Guo, H., Ling, Z. H., Cheung, K., Wang, D. W., Simpson, I. J., and Blake, D. R.: Acetone in the atmosphere of Hong Kong: Abundance, sources and photochemical precursors, *Atmos. Environ.*, 65, 80-88, <https://doi.org/10.1016/j.atmosenv.2012.10.027>, 2013.
- Guo, J., Xu, Q., Yu, S., Zhao, B., and Zhang, M.: Investigation of atmospheric VOCs sources and ozone formation sensitivity during epidemic closure and control: A case study of Zhengzhou, *Atmos. Pollut. Res.*, 15, <https://doi.org/10.1016/j.apr.2023.102035>, 2024.
- He, Z., Li, G., Chen, J., Huang, Y., An, T., and Zhang, C.: Pollution characteristics and health risk assessment of volatile organic compounds emitted from different plastic solid waste recycling workshops, *Environ.*

653 Int., 77, 85-94, <https://doi.org/10.1016/j.envint.2015.01.004>, 2015.

654 Hong, Z., Li, M., Wang, H., Xu, L., Hong, Y., Chen, J., Chen, J., Zhang, H., Zhang, Y., Wu, X., Hu, B., and  
655 Li, M.: Characteristics of atmospheric volatile organic compounds (VOCs) at a mountainous forest site  
656 and two urban sites in the southeast of China, *Sci. Total. Environ.*, 657, 1491-1500,  
657 <https://doi.org/10.1016/j.scitotenv.2018.12.132>, 2019.

658 Huang, B., Lei, C., Wei, C., and Zeng, G.: Chlorinated volatile organic compounds (Cl-VOCs) in environment  
659 — sources, potential human health impacts, and current remediation technologies, *Environ. Int.*, 71, 118-  
660 138, <https://doi.org/10.1016/j.envint.2014.06.013>, 2014.

661 Huang, C., Shi, Y., Yang, M., Tong, L., Dai, X., Liu, F., Huang, C., Zheng, J., Li, J., and Xiao, H.:  
662 Spatiotemporal distribution, source apportionment and health risk assessment of atmospheric volatile  
663 organic compounds using passive air samplers in a typical coastal area, China, *J. Clean. Prod.*, 423,  
664 138741, <https://doi.org/10.1016/j.jclepro.2023.138741>, 2023.

665 Huang, J., Fung, J. C. H., Lau, A. K. H., and Qin, Y.: Numerical simulation and process analysis of typhoon-  
666 related ozone episodes in Hong Kong, *J. Geophys. Res-Atmos.*, 110,  
667 <https://doi.org/10.1029/2004jd004914>, 2005.

668 Hui, L., Ma, T., Gao, Z., Gao, J., Wang, Z., Xue, L., Liu, H., and Liu, J.: Characteristics and sources of volatile  
669 organic compounds during high ozone episodes: A case study at a site in the eastern Guanzhong Plain,  
670 China, *Chemosphere*, 265, 129072, <https://doi.org/10.1016/j.chemosphere.2020.129072>, 2020.

671 Jorquera, H., and Rappenglück, B.: Receptor modeling of ambient VOC at Santiago, Chile, *Atmos. Environ.*,  
672 38, 4243-4263, <https://doi.org/10.1016/j.atmosenv.2004.04.030>, 2004.

673 Kim, E., and Hopke, P.: Comparison between conditional probability function and nonparametric regression  
674 for fine particle source directions, *Atmos. Environ.*, 38, 4667-4673,  
675 <https://doi.org/10.1016/j.atmosenv.2004.05.035>, 2004.

676 Kleinman, L. I.: Ozone process insights from field experiments – part II: Observation-based analysis for ozone  
677 production, *Atmos. Environ.*, 34, 2023-2033, [https://doi.org/https://doi.org/10.1016/S1352-  
678 2310\(99\)00457-4](https://doi.org/10.1016/S1352-2310(99)00457-4), 2000.

679 Lerner, J. E. C., Sanchez, E. Y., Sambeth, J. E., and Porta, A. A.: Characterization and health risk assessment  
680 of VOCs in occupational environments in Buenos Aires, Argentina, *Atmos. Environ.*, 55, 440-447,  
681 <https://doi.org/10.1016/j.atmosenv.2012.03.041>, 2012.

682 Li, J., Zhai, C., Yu, J., Liu, R., Li, Y., Zeng, L., and Xie, S.: Spatiotemporal variations of ambient volatile  
683 organic compounds and their sources in Chongqing, a mountainous megacity in China, *Sci. Total.*



684 Environ., 627, 1442-1452, <https://doi.org/10.1016/j.scitotenv.2018.02.010>, 2018.

685 Li, Y., Wu, Z., Ji, Y., Chen, T., Li, H., Gao, R., Xue, L., Wang, Y., Zhao, Y., and Yang, X.: Comparison of the  
686 ozone formation mechanisms and VOCs apportionment in different ozone pollution episodes in urban  
687 Beijing in 2019 and 2020: Insights for ozone pollution control strategies, *Sci. Total. Environ.*, 908,  
688 <https://doi.org/10.1016/j.scitotenv.2023.168332>, 2024.

689 Li, Y., Yin, S., Yu, S., Yuan, M., Dong, Z., Zhang, D., Yang, L., and Zhang, R.: Characteristics, source  
690 apportionment and health risks of ambient VOCs during high ozone period at an urban site in central plain,  
691 China, *Chemosphere*, 250, 126283, <https://doi.org/10.1016/j.chemosphere.2020.126283>, 2020.

692 Lin, C., Ho, T. C., Chu, H., Yang, H., Chandru, S., Krishnarajanagar, N., Chiou, P., and Hopper, J. R.:  
693 Sensitivity analysis of ground-level ozone concentration to emission changes in two urban regions of  
694 southeast Texas, *J. Environ. Manage.*, 75, 315-323, <https://doi.org/10.1016/j.jenvman.2004.09.012>, 2005.

695 Ling, Z. H., Guo, H., Cheng, H. R., and Yu, Y. F.: Sources of ambient volatile organic compounds and their  
696 contributions to photochemical ozone formation at a site in the Pearl River Delta, southern China, *Environ.*  
697 *Pollut.*, 159, 2310-2319, <https://doi.org/10.1016/j.envpol.2011.05.001>, 2011.

698 Ling, Z. H., Guo, H., Zheng, J. Y., Louie, P. K. K., Cheng, H. R., Jiang, F., Cheung, K., Wong, L. C., and Feng,  
699 X. Q.: Establishing a conceptual model for photochemical ozone pollution in subtropical Hong Kong,  
700 *Atmos. Environ.*, 76, 208-220, <https://doi.org/10.1016/j.atmosenv.2012.09.051>, 2013.

701 Liu, B., Liang, D., Yang, J., Dai, Q., Bi, X., Feng, Y., Yuan, J., Xiao, Z., Zhang, Y., and Xu, H.: Characterization  
702 and source apportionment of volatile organic compounds based on 1-year of observational data in Tianjin,  
703 China, *Environ. Pollut.*, 218, 757-769, <https://doi.org/10.1016/j.envpol.2016.07.072>, 2016.

704 Liu, B., Yang, Y., Yang, T., Dai, Q., Zhang, Y., Feng, Y., and Hopke, P. K.: Effect of photochemical losses of  
705 ambient volatile organic compounds on their source apportionment, *Environ. Int.*, 172, 107766,  
706 <https://doi.org/10.1016/j.envint.2023.107766>, 2023a.

707 Liu, T., Hong, Y., Li, M., Xu, L., Chen, J., Bian, Y., Yang, C., Dan, Y., Zhang, Y., Xue, L., Zhao, M., Huang,  
708 Z., and Wang, H.: Atmospheric oxidation capacity and ozone pollution mechanism in a coastal city of  
709 southeastern China: analysis of a typical photochemical episode by an observation-based model, *Atmos.*  
710 *Chem. Phys.*, 22, 2173-2190, <https://doi.org/10.5194/acp-22-2173-2022>, 2022.

711 Liu, Y., Shao, M., Fu, L., Lu, S., Zeng, L., and Tang, D.: Source profiles of volatile organic compounds (VOCs)  
712 measured in China: Part I, *Atmos. Environ.*, 42, 6247-6260,  
713 <https://doi.org/10.1016/j.atmosenv.2008.01.070>, 2008.

714 Liu, Y., Song, M., Liu, X., Zhang, Y., Hui, L., Kong, L., Zhang, Y., Zhang, C., Qu, Y., An, J., Ma, D., Tan, Q.,

- 715 and Feng, M.: Characterization and sources of volatile organic compounds (VOCs) and their related  
716 changes during ozone pollution days in 2016 in Beijing, China, *Environ. Pollut.*, 257, 113599,  
717 <https://doi.org/10.1016/j.envpol.2019.113599>, 2020.
- 718 Liu, Y., Kong, L., Liu, X., Zhang, Y., Li, C., Zhang, Y., Zhang, C., Qu, Y., An, J., Ma, D., Tan, Q., Feng, M.,  
719 and Zha, S.: Characteristics, secondary transformation, and health risk assessment of ambient volatile  
720 organic compounds (VOCs) in urban Beijing, China, *Atmos. Pollut. Res.*, 12, 33-46,  
721 <https://doi.org/10.1016/j.apr.2021.01.013>, 2021.
- 722 Liu, Z., Hu, K., Zhang, K., Zhu, S., Wang, M., and Li, L.: VOCs sources and roles in O<sub>3</sub> formation in the  
723 central Yangtze River Delta region of China, *Atmos. Environ.*, 302, 119755,  
724 <https://doi.org/10.1016/j.atmosenv.2023.119755>, 2023b.
- 725 Liu, Z., Wang, B., Wang, C., Sun, Y., Zhu, C., Sun, L., Yang, N., Fan, G., Sun, X., Xia, Z., Pan, G., Zhu, C.,  
726 Gai, Y., Wang, X., Xiao, Y., Yan, G., and Xu, C.: Characterization of photochemical losses of volatile  
727 organic compounds and their implications for ozone formation potential and source apportionment during  
728 summer in suburban Jinan, China, *Environ. Res.*, 238, 117158,  
729 <https://doi.org/10.1016/j.envres.2023.117158>, 2023c.
- 730 Lu, B., Zhang, Z., Jiang, J., Meng, X., Liu, C., Herrmann, H., Chen, J., Xue, L., and Li, X.: Unraveling the  
731 O<sub>3</sub>-NO<sub>x</sub>-VOCs relationships induced by anomalous ozone in industrial regions during COVID-19 in  
732 Shanghai, *Atmos. Environ.*, 308, 119864, <https://doi.org/10.1016/j.atmosenv.2023.119864>, 2023.
- 733 Lyu, X. P., Chen, N., Guo, H., Zhang, W. H., Wang, N., Wang, Y., and Liu, M.: Ambient volatile organic  
734 compounds and their effect on ozone production in Wuhan, central China, *Sci. Total. Environ.*, 541, 200-  
735 209, <https://doi.org/10.1016/j.scitotenv.2015.09.093>, 2016.
- 736 Meng, X., Jiang, J., Chen, T., Zhang, Z., Lu, B., Liu, C., Xue, L., Chen, J., Herrmann, H., and Li, X.: Chemical  
737 drivers of ozone change in extreme temperatures in eastern China, *Sci. Total. Environ.*, 874,  
738 <https://doi.org/10.1016/j.scitotenv.2023.162424>, 2023.
- 739 Meng, Y., Song, J., Zeng, L., Zhang, Y., Zhao, Y., Liu, X., Guo, H., Zhong, L., Ou, Y., Zhou, Y., Zhang, T.,  
740 Yue, D., and Lai, S.: Ambient volatile organic compounds at a receptor site in the Pearl River Delta region:  
741 Variations, source apportionment and effects on ozone formation, *J. Environ. Sci.*, 111, 104-117,  
742 <https://doi.org/10.1016/j.jes.2021.02.024>, 2022.
- 743 Miller, L., Xu, X., Grgicak-Mannion, A., Brook, J., and Wheeler, A.: Multi-season, multi-year concentrations  
744 and correlations amongst the BTEX group of VOCs in an urbanized industrial city, *Atmos. Environ.*, 61,  
745 305-315, <https://doi.org/10.1016/j.atmosenv.2012.07.041>, 2012.

- 746 Min, R., Wang, F., Wang, Y., Song, G., Zheng, H., Zhang, H., Ru, X., and Song, H.: Contribution of local and  
747 surrounding area anthropogenic emissions to a high ozone episode in Zhengzhou, China, *Environ. Res.*,  
748 212, 113440, <https://doi.org/10.1016/j.envres.2022.113440>, 2022.
- 749 Ministry of Environmental Protection of China, 2012. Ambient air quality standards. (GB 3095-2012).  
750 <https://www.mee.gov.cn/ywgz/fgbz/bz/bzwb/dqhjbh/dqhjzlbz/201203/W020120410330232398521.pdf>.
- 751 Ming, W., Wentai, C., Lin, Z., Wei, Q., Yong, Z., Xiangzhi, Z., and Xin, X.: Ozone pollution characteristics  
752 and sensitivity analysis using an observation-based model in Nanjing, Yangtze River Delta Region of  
753 China, *J. Environ. Sci.*, <https://doi.org/10.1016/j.jes.2020.02.027>, 2020.
- 754 Mo, Z., Shao, M., Lu, S., Qu, H., Zhou, M., Sun, J., and Gou, B.: Process-specific emission characteristics of  
755 volatile organic compounds (VOCs) from petrochemical facilities in the Yangtze River Delta, China, *Sci.*  
756 *Total. Environ.*, 533, 422-431, <https://doi.org/10.1016/j.scitotenv.2015.06.089>, 2015.
- 757 Monod, A., Sive, B. C., Avino, P., Chen, T., Blake, D. R., and Sherwood Rowland, F.: Monoaromatic  
758 compounds in ambient air of various cities: a focus on correlations between the xylenes and ethylbenzene,  
759 *Atmos. Environ.*, 35, 135-149, [https://doi.org/https://doi.org/10.1016/S1352-2310\(00\)00274-0](https://doi.org/https://doi.org/10.1016/S1352-2310(00)00274-0), 2001.
- 760 Mozaffar, A., Zhang, Y., Fan, M., Cao, F., and Lin, Y.: Characteristics of summertime ambient VOCs and their  
761 contributions to O<sub>3</sub> and SOA formation in a suburban area of Nanjing, China, *Atmos. Res.*, 240, 104923,  
762 <https://doi.org/10.1016/j.atmosres.2020.104923>, 2020.
- 763 Mozaffar, A., Zhang, Y., Lin, Y., Xie, F., Fan, M., and Cao, F.: Measurement report: High contributions of  
764 halocarbon and aromatic compounds to atmospheric volatile organic compounds in an industrial area,  
765 *Atmos. Chem. Phys.*, 21, 18087-18099, <https://doi.org/10.5194/acp-21-18087-2021>, 2021.
- 766 MPS (The Ministry of Public Security of the People's Republic of China), 2022. The number of motor vehicles  
767 in China exceeded 400 million. <https://www.mps.gov.cn/n2254314/n6409334/c8451247/content.html>.  
768 (Accessed 10 October 2023).
- 769 Na, K., Kim, Y. P., Moon, K.-C., Moon, I., and Fung, K.: Concentrations of volatile organic compounds in an  
770 industrial area of Korea, *Atmos. Environ.*, 35, 2747-2756, [https://doi.org/https://doi.org/10.1016/S1352-](https://doi.org/https://doi.org/10.1016/S1352-2310(00)00313-7)  
771 [2310\(00\)00313-7](https://doi.org/https://doi.org/10.1016/S1352-2310(00)00313-7), 2001.
- 772 Nelson, B. S., Stewart, G. J., Drysdale, W. S., Newland, M. J., Vaughan, A. R., Dunmore, R. E., Edwards, P.  
773 M., Lewis, A. C., Hamilton, J. F., and Acton, W. J.: In situ ozone production is highly sensitive to volatile  
774 organic compounds in Delhi, India, *Copernicus Publications*, 17, [https://doi.org/10.5194/ACP-21-13609-](https://doi.org/10.5194/ACP-21-13609-2021)  
775 [2021](https://doi.org/10.5194/ACP-21-13609-2021), 2021.
- 776 Nopmongcol, U., Koo, B., Tai, E., Jung, J., Piyachaturawat, P., Emery, C., Yarwood, G., Pirovano, G.,

- 777 Mitsakou, C., and Kallos, G.: Modeling Europe with CAMx for the Air Quality Model Evaluation  
778 International Initiative (AQMEII), *Atmos. Environ.*, 53, 177-185,  
779 <https://doi.org/https://doi.org/10.1016/j.atmosenv.2011.11.023>, 2012.
- 780 Norris, G., Duvall, R., Brown, S., and Bai, S.: EPA Positive Matrix Factorization (PMF) 5.0. Fundamentals  
781 and User Guide Prepared for the U.S. Environmental Protection Agency Office of Research and  
782 Development, Washington, DC (EPA/600/R-14/108; STI-9105115594-UG, April), 2014.
- 783 Pacifico, F., Harrison, S. P., Jones, C. D., and Sitch, S.: Isoprene emissions and climate, *Atmos. Environ.*, 43,  
784 6121-6135, <https://doi.org/10.1016/j.atmosenv.2009.09.002>, 2009.
- 785 Prendez, M., Carvajal, V., Corada, K., Morales, J., Alarcon, F., and Peralta, H.: Biogenic volatile organic  
786 compounds from the urban forest of the Metropolitan Region, Chile, *Environ. Pollut.*, 183, 143-150,  
787 <https://doi.org/10.1016/j.envpol.2013.04.003>, 2013.
- 788 Qiao, X., Sun, M., Wang, Y., Zhang, D., Zhang, R., Zhao, B., and Zhang, J.: Strong relations of peroxyacetyl  
789 nitrate (PAN) formation to alkene and nitrous acid during various episodes, *Environ. Pollut.*, 326, 121465,  
790 <https://doi.org/10.1016/j.envpol.2023.121465>, 2023.
- 791 Qin, J., Wang, X., Yang, Y., Qin, Y., Shi, S., Xu, P., Chen, R., Zhou, X., Tan, J., and Wang, X.: Source  
792 apportionment of VOCs in a typical medium-sized city in North China Plain and implications on control  
793 policy, *J. Environ. Sci.*, 107, 26-37, <https://doi.org/10.1016/j.jes.2020.10.005>, 2021.
- 794 Qin, Z., Xu, B., Zheng, Z., Li, L., Zhang, G., Li, S., Geng, C., Bai, Z., and Yang, W.: Integrating ambient  
795 carbonyl compounds provides insight into the constrained ozone formation chemistry in Zibo city of the  
796 North China Plain, *Environ. Pollut.*, 324, <https://doi.org/10.1016/j.envpol.2023.121294>, 2023.
- 797 Ring, A. M., Canty, T. P., Anderson, D. C., Vinciguerra, T. P., He, H., Goldberg, D. L., Ehrman, S. H.,  
798 Dickerson, R. R., and Salawitch, R. J.: Evaluating commercial marine emissions and their role in air  
799 quality policy using observations and the CMAQ model, *Atmos. Environ.*, 173, 96-107,  
800 <https://doi.org/10.1016/j.atmosenv.2017.10.037>, 2018.
- 801 Seila, R. L., Main, H. H., Arriaga, J. L., Martínez V, G., and Ramadan, A. B.: Atmospheric volatile organic  
802 compound measurements during the 1996 Paso del Norte Ozone Study, *Sci. Total. Environ.*, 276, 153-  
803 169, [https://doi.org/https://doi.org/10.1016/S0048-9697\(01\)00777-X](https://doi.org/https://doi.org/10.1016/S0048-9697(01)00777-X), 2001.
- 804 Sha, Q., Zhu, M., Huang, H., Wang, Y., Huang, Z., Zhang, X., Tang, M., Lu, M., Chen, C., Shi, B., Chen, Z.,  
805 Wu, L., Zhong, Z., Li, C., Xu, Y., Yu, F., Jia, G., Liao, S., Cui, X., Liu, J., and Zheng, J.: A newly integrated  
806 dataset of volatile organic compounds (VOCs) source profiles and implications for the future development  
807 of VOCs profiles in China, *Sci. Total. Environ.*, 793, 148348,

808 <https://doi.org/10.1016/j.scitotenv.2021.148348>, 2021.

809 Shao, M., Zhang, Y., Zeng, L., Tang, X., Zhang, J., Zhong, L., and Wang, B.: Ground-level ozone in the Pearl  
810 River Delta and the roles of VOC and NO(x) in its production, *J. Environ. Manage.*, 90, 512-518,  
811 <https://doi.org/10.1016/j.jenvman.2007.12.008>, 2009.

812 Shao, P., An, J., Xin, J., Wu, F., Wang, J., Ji, D., and Wang, Y.: Source apportionment of VOCs and the  
813 contribution to photochemical ozone formation during summer in the typical industrial area in the Yangtze  
814 River Delta, China, *Atmos. Res.*, 176-177, 64-74, <https://doi.org/10.1016/j.atmosres.2016.02.015>, 2016.

815 Sicard, P., De Marco, A., Agathokleous, E., Feng, Z., Xu, X., Paoletti, E., Rodriguez, J. J. D., and Calatayud,  
816 V.: Amplified ozone pollution in cities during the COVID-19 lockdown, *Sci. Total. Environ.*, 735, 139542,  
817 <https://doi.org/10.1016/j.scitotenv.2020.139542>, 2020.

818 Sillman, S.: The relation between ozone, NO<sub>x</sub> and hydrocarbons in urban and polluted rural environments,  
819 *Atmos. Environ.*, 33, 1821–1845, [https://doi.org/https://doi.org/10.1016/S1352-2310\(98\)00345-8](https://doi.org/https://doi.org/10.1016/S1352-2310(98)00345-8), 1999.

820 Song, Y., Shao, M., Liu, Y., Lu, S., Kuster, W., Goldan, P., and Xie, S.: Source apportionment of ambient  
821 volatile organic compounds in Beijing, *Environ. Sci. Technol.*, 41, 4348-4353, 2007.

822 Tang, J. H., Chan, L. Y., Chan, C. Y., Li, Y. S., Chang, C. C., Liu, S. C., Wu, D., and Li, Y. D.: Characteristics  
823 and diurnal variations of NMHCs at urban, suburban, and rural sites in the Pearl River Delta and a remote  
824 site in South China, *Atmos. Environ.*, 41, 8620-8632, <https://doi.org/10.1016/j.atmosenv.2007.07.029>,  
825 2007.

826 Thijssen, T. R., Oss, R. F. V., and Lenschow, P.: Determination of Source Contributions to Ambient Volatile  
827 Organic Compound Concentrations in Berlin, *J. Air. Waste. Manage.*, 49, 1394-1404,  
828 <https://doi.org/10.1080/10473289.1999.10463974>, 1999.

829 Tsai, W. Y., Chan, L. Y., Blake, D. R., and Chu, K. W.: Vehicular fuel composition and atmospheric emissions  
830 in South China: Hong Kong, Macau, Guangzhou, and Zhuhai, *Atmos. Chem. Phys.*, 6, 3281-3288,  
831 <https://doi.org/10.5194/acp-6-3281-2006>, 2006.

832 Uria-Tellaetxe, I., and Carslaw, D. C.: Conditional bivariate probability function for source identification,  
833 *Environ. Modell. Softw.*, 59, 1-9, <https://doi.org/10.1016/j.envsoft.2014.05.002>, 2014.

834 Positive Matrix Factorization Model for environmental data analyses: <https://www.epa.gov/air-research/positive-matrix-factorization-model-environmental-data-analyses>, access: June, 2014.

835

836 Wang, B., Liu, Z., Li, Z., Sun, Y., Wang, C., Zhu, C., Sun, L., Yang, N., Bai, G., Fan, G., Sun, X., Xia, Z., Pan,  
837 G., Xu, C., and Yan, G.: Characteristics, chemical transformation and source apportionment of volatile  
838 organic compounds (VOCs) during wintertime at a suburban site in a provincial capital city, east China,

839 Atmos. Environ., 298, 119621, <https://doi.org/10.1016/j.atmosenv.2023.119621>, 2023a.

840 Wang, M., Sheng, H., Liu, Y., Wang, G., Huang, H., Fan, L., and Ye, D.: Research on the diurnal variation  
841 characteristics of ozone formation sensitivity and the impact of ozone pollution control measures in "2 +  
842 26" cities of Henan Province in summer, *Sci. Total. Environ.*, 888, 164121,  
843 <https://doi.org/10.1016/j.scitotenv.2023.164121>, 2023b.

844 Wang, P., Chen, Y., Hu, J., Zhang, H., and Ying, Q.: Source apportionment of summertime ozone in China  
845 using a source-oriented chemical transport model, *Atmos. Environ.*, 211, 79-90,  
846 <https://doi.org/10.1016/j.atmosenv.2019.05.006>, 2019.

847 Wang, X., Yin, S., Zhang, R., Yuan, M., and Ying, Q.: Assessment of summertime O<sub>3</sub> formation and the O<sub>3</sub>-  
848 NO<sub>x</sub>-VOC sensitivity in Zhengzhou, China using an observation-based model, *Sci. Total. Environ.*, 813,  
849 152449, <https://doi.org/10.1016/j.scitotenv.2021.152449>, 2022.

850 Wang, Y., Guo, H., Zou, S., Lyu, X., Ling, Z., Cheng, H., and Zeren, Y.: Surface O<sub>3</sub> photochemistry over the  
851 South China Sea: Application of a near-explicit chemical mechanism box model, *Environ. Pollut.*, 234,  
852 155-166, <https://doi.org/10.1016/j.envpol.2017.11.001>, 2018.

853 Wang, Y., Wang, H., Guo, H., Lyu, X., Cheng, H., Ling, Z., Louie, P. K. K., Simpson, I. J., Meinardi, S., and  
854 Blake, D. R.: Long-term O<sub>3</sub>-precursor relationships in Hong Kong: field observation and model  
855 simulation, *Atmos. Chem. Phys.*, 17, 10919-10935, <https://doi.org/10.5194/acp-17-10919-2017>, 2017.

856 Watson, J. G., Chow, J. C., and Fujita, E. M.: Review of volatile organic compound source apportionment by  
857 chemical mass balance, *Atmos. Environ.*, 35, 1567-1584, [https://doi.org/10.1016/S1352-2310\(00\)00461-](https://doi.org/10.1016/S1352-2310(00)00461-1)  
858 1, 2001.

859 Wu, R., Li, J., Hao, Y., Li, Y., Zeng, L., and Xie, S.: Evolution process and sources of ambient volatile organic  
860 compounds during a severe haze event in Beijing, China, *Sci. Total. Environ.*, 560-561, 62-72,  
861 <https://doi.org/10.1016/j.scitotenv.2016.04.030>, 2016.

862 Wu, Y., Fan, X., Liu, Y., Zhang, J., Wang, H., Sun, L., Fang, T., Mao, H., Hu, J., Wu, L., Peng, J., and Wang,  
863 S.: Source apportionment of VOCs based on photochemical loss in summer at a suburban site in Beijing,  
864 *Atmos. Environ.*, 293, <https://doi.org/10.1016/j.atmosenv.2022.119459>, 2023.

865 Wu, Y., Liu, B., Meng, H., Dai, Q., Shi, L., Song, S., Feng, Y., and Hopke, P. K.: Changes in source apportioned  
866 VOCs during high O<sub>3</sub> periods using initial VOC-concentration-dispersion normalized PMF, *Sci. Total.*  
867 *Environ.*, 896, <https://doi.org/10.1016/j.scitotenv.2023.165182>, 2023.

868 Xia, L., Cai, C., Zhu, B., An, J., Li, Y., and Li, Y.: Source apportionment of VOCs in a suburb of Nanjing,  
869 China, in autumn and winter, *J. Atmos. Chem.*, 71, 175-193, <https://doi.org/10.1007/s10874-014-9289-6>,



870 2014.

871 Xie, Y., and Berkowitz, C. M.: The use of positive matrix factorization with conditional probability functions  
872 in air quality studies: An application to hydrocarbon emissions in Houston, Texas, *Atmos. Environ.*, 40,  
873 3070-3091, <https://doi.org/10.1016/j.atmosenv.2005.12.065>, 2006.

874 Xie, Y., Cheng, C., Wang, Z., Wang, K., Wang, Y., Zhang, X., Li, X., Ren, L., Liu, M., and Li, M.: Exploration  
875 of O<sub>3</sub>-precursor relationship and observation-oriented O<sub>3</sub> control strategies in a non-provincial capital city,  
876 southwestern China, *Sci. Total. Environ.*, 800, 149422, <https://doi.org/10.1016/j.scitotenv.2021.149422>,  
877 2021.

878 Xu, Z., Zou, Q., Jin, L., Shen, Y., Shen, J., Xu, B., Qu, F., Zhang, F., Xu, J., Pei, X., Xie, G., Kuang, B., Huang,  
879 X., Tian, X., and Wang, Z.: Characteristics and sources of ambient Volatile Organic Compounds (VOCs)  
880 at a regional background site, YRD region, China: Significant influence of solvent evaporation during hot  
881 months, *Sci. Total. Environ.*, 857, 159674, <https://doi.org/10.1016/j.scitotenv.2022.159674>, 2023.

882 Yan, D., Zhang, Z., Jin, Z., Li, M., Sheridan, S. C., and Wang, T.: Ozone variability driven by the synoptic  
883 patterns over China during 2014–2022 and its implications for crop yield and economy, *Atmos. Pollut.*  
884 *Res.*, 14, 101843, <https://doi.org/10.1016/j.apr.2023.101843>, 2023.

885 Yang, L., Yuan, Z., Luo, H., Wang, Y., Xu, Y., Duan, Y., and Fu, Q.: Identification of long-term evolution of  
886 ozone sensitivity to precursors based on two-dimensional mutual verification, *Sci. Total. Environ.*, 760,  
887 143401, <https://doi.org/10.1016/j.scitotenv.2020.143401>, 2021.

888 Yu, S., Su, F., Yin, S., Wang, S., Xu, R., He, B., Fan, X., Yuan, M., and Zhang, R.: Characterization of ambient  
889 volatile organic compounds, source apportionment, and the ozone-NO<sub>x</sub>-VOC sensitivities in a heavily  
890 polluted megacity of central China: effect of sporting events and emission reductions, *Atmos. Chem. Phys.*,  
891 21, 15239-15257, <https://doi.org/10.5194/acp-21-15239-2021>, 2021.

892 Yu, S., Wang, S., Xu, R., Zhang, D., Zhang, M., Su, F., Lu, X., Li, X., Zhang, R., and Wang, L.: Measurement  
893 report: Intra- and interannual variability and source apportionment of volatile organic compounds during  
894 2018–2020 in Zhengzhou, central China, *Atmos. Chem. Phys.*, 22, 14859-14878,  
895 <https://doi.org/10.5194/acp-22-14859-2022>, 2022.

896 Yuan, B., Shao, M., de Gouw, J., Parrish, D. D., Lu, S., Wang, M., Zeng, L., Zhang, Q., Song, Y., Zhang, J.,  
897 and Hu, M.: Volatile organic compounds (VOCs) in urban air: How chemistry affects the interpretation  
898 of positive matrix factorization (PMF) analysis, *J. Geophys. Res-Atmos.*, 117, 24302,  
899 <https://doi.org/10.1029/2012jd018236>, 2012.

900 Yuan, Z., Zhong, L., Lau, A. K. H., Yu, J. Z., and Louie, P. K. K.: Volatile organic compounds in the Pearl

- 901 River Delta: Identification of source regions and recommendations for emission-oriented monitoring  
902 strategies, *Atmos. Environ.*, 76, 162-172, <https://doi.org/10.1016/j.atmosenv.2012.11.034>, 2013.
- 903 Yurdakul, S., Civan, M., Kuntasal, Ö., Doğan, G., Pekey, H., and Tuncel, G.: Temporal variations of VOC  
904 concentrations in Bursa atmosphere, *Atmos. Pollut. Res.*, 9, 189-206,  
905 <https://doi.org/10.1016/j.apr.2017.09.004>, 2018.
- 906 Zeng, X., Han, M., Ren, G., Liu, G., Wang, X., Du, K., Zhang, X., and Lin, H.: A comprehensive investigation  
907 on source apportionment and multi-directional regional transport of volatile organic compounds and  
908 ozone in urban Zhengzhou, *Chemosphere*, 334, 139001,  
909 <https://doi.org/10.1016/j.chemosphere.2023.139001>, 2023.
- 910 Zhang, D., He, B., Yuan, M., Yu, S., Yin, S., and Zhang, R.: Characteristics, sources and health risks  
911 assessment of VOCs in Zhengzhou, China during haze pollution season, *J. Environ. Sci.*, 108, 44-57,  
912 <https://doi.org/10.1016/j.jes.2021.01.035>, 2021.
- 913 Zhang, H., Wang, Y., Hu, J., Ying, Q., and Hu, X. M.: Relationships between meteorological parameters and  
914 criteria air pollutants in three megacities in China, *Environ. Res.*, 140, 242-254,  
915 <https://doi.org/10.1016/j.envres.2015.04.004>, 2015.
- 916 Zhang, L., Li, H., Wu, Z., Zhang, W., Liu, K., Cheng, X., Zhang, Y., Li, B., and Chen, Y.: Characteristics of  
917 atmospheric volatile organic compounds in urban area of Beijing: Variations, photochemical reactivity  
918 and source apportionment, *J. Environ. Sci.*, 95, 190-200, <https://doi.org/10.1016/j.jes.2020.03.023>, 2020.
- 919 Zhang, Y., Li, R., Fu, H., Zhou, D., and Chen, J.: Observation and analysis of atmospheric volatile organic  
920 compounds in a typical petrochemical area in Yangtze River Delta, China, *J. Environ. Sci.*, 71, 233-248,  
921 <https://doi.org/10.1016/j.jes.2018.05.027>, 2018.
- 922 Zhang, Y. H., Su, H., Zhong, L. J., Cheng, Y. F., Zeng, L. M., Wang, X. S., Xiang, Y. R., Wang, J. L., Gao, D.  
923 F., and Shao, M.: Regional ozone pollution and observation-based approach for analyzing ozone–  
924 precursor relationship during the PRIDE-PRD2004 campaign, *Atmos. Environ.*, 42, 6203-6218,  
925 <https://doi.org/10.1016/j.atmosenv.2008.05.002>, 2008.
- 926 Zhang, Z., Zhang, Y., Wang, X., Lü, S., Huang, Z., Huang, X., Yang, W., Wang, Y., and Zhang, Q.:  
927 Spatiotemporal patterns and source implications of aromatic hydrocarbons at six rural sites across China's  
928 developed coastal regions, *J. Geophys. Res-Atmos.*, 121, 6669-6687,  
929 <https://doi.org/10.1002/2016jd025115>, 2016.
- 930 Zhang, Z., Sun, Y., and Li, J.: Characteristics and sources of VOCs in a coastal city in eastern China and the  
931 implications in secondary organic aerosol and O<sub>3</sub> formation, *Sci. Total. Environ.*, 887, 164117,

- 932 <https://doi.org/10.1016/j.scitotenv.2023.164117>, 2023.
- 933 Zhao, C., Sun, Y., Zhong, Y., Xu, S., Liang, Y., Liu, S., He, X., Zhu, J., Shibamoto, T., and He, M.: Spatio-  
934 temporal analysis of urban air pollutants throughout China during 2014-2019, *Air. Qual. Atmos. Hlth.*, 14,  
935 1619-1632, <https://doi.org/10.1007/s11869-021-01043-5>, 2021.
- 936 Zhao, Y., Chen, L., Li, K., Han, L., Zhang, X., Wu, X., Gao, X., Azzi, M., and Cen, K.: Atmospheric ozone  
937 chemistry and control strategies in Hangzhou, China: Application of a 0-D box model, *Atmos. Res.*, 246,  
938 <https://doi.org/10.1016/j.atmosres.2020.105109>, 2020.
- 939 Zhu, B., Huang, X., Xia, S., Lin, L., Cheng, Y., and He, L.: Biomass-burning emissions could significantly  
940 enhance the atmospheric oxidizing capacity in continental air pollution, *Environ. Pollut.*, 285, 117523,  
941 <https://doi.org/10.1016/j.envpol.2021.117523>, 2021.
- 942 Zong, R., Yang, X., Wen, L., Xu, C., Zhu, Y., Chen, T., Yao, L., Wang, L., Zhang, J., Yang, L., Wang, X., Shao,  
943 M., Zhu, T., Xue, L., and Wang, W.: Strong ozone production at a rural site in the North China Plain:  
944 Mixed effects of urban plumes and biogenic emissions, *J. Environ. Sci.*, 71, 261-270,  
945 <https://doi.org/10.1016/j.jes.2018.05.003>, 2018.
- 946 Zou, Y., Yan, X. L., Flores, R. M., Zhang, L. Y., Yang, S. P., Fan, L. Y., Deng, T., Deng, X. J., and Ye, D. Q.:  
947 Source apportionment and ozone formation mechanism of VOCs considering photochemical loss in  
948 Guangzhou, China, *Sci. Total. Environ.*, 903, 166191, <https://doi.org/10.1016/j.scitotenv.2023.166191>,  
949 2023.

950  
951